Abubaker Shabbir [240062858], Madeleine Bell, Dawood Tahir, Gerard Hyseni

CW1 Quanser Helicopter - EPM103

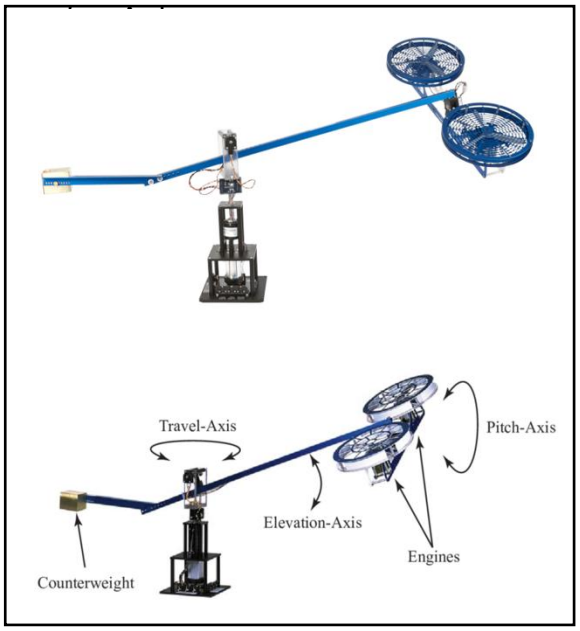

The 3 DOF Quanser Helicopter experiment provides an affordable platform for analysing and designing control laws for vehicles with dynamics similar dual rotor rigid body helicopter (Quanser,2023). This project involves designing a control system for a Quanser Helicopter, simulating a scenario where it functions as a reduced DOF helicopter.

Stage 1: Analyse the helicopter's physical model - Create a fast & stable roll controller as the "inner-loop" for travel control - Accommodating for variations in pitch and roll damping.

Stage 2: Develop a travel controller to command the roll angle, ensuring smooth horizontal travel (with voltage constraints of ± 5V).

(Fig.1., *3 DOF helicopter - Quanser*, 2023)

Nomenclature

$\dot{\psi}$ — Rate of change in the yaw angle

ϕ — Roll Angle

τ_{coll} — Collective torque, used for thrust control

l_{boom} — Length from the pivot point to the helicopter body

M — Mass of the whole setup

D — Induced Drag

T_{cyc} — cyclic thrust

ω_{coll} — collective rotor speed

γ — Vehicles Flight Path Angle

I_{xx} — Moment of inertia about the x-axis.

I_{yy} — Moment of inertia about the y-axis.

I_{zz} — Moment of inertia about the z-axis.

$\ddot{\phi}$ — Angular acceleration in roll (φ) axis.

$\ddot{\theta}$ — Angular acceleration in pitch (θ) axis.

l_θ — length of the pendulum for the pitch axis

γ — Angle/gain factor related to flight dynamics.

V_{cyc} - cyclic voltage

K_D — Drag Coefficient

$\ddot{\psi}$ – Angular acceleration in the yaw (ψ) axis.

τ_{cyc} — Cyclic torque applied for controlling roll and pitch.

l_h — Length from the pivot point to the rotor

m — Mass of the rotor assembly

g — Gravitational acceleration

θ — Pitch angle of the helicopter

M_q — pitch damping coefficient

V_{coll} — collective voltage

K_T — Drag Coefficient

l_ϕ — Length of the pendulum for the roll axis

L_p — roll damping coefficient

I_R — Distance to the rotor or effective rotor arm length

ω_{rotor} — Rotor angular velocity

$\dot{\theta}$ - Angular velocity in the pitch axis

θ_{rest} — Resting/ equilibrium pitch angle

T_{coll} — collective thrust

ω_{cyc} — cyclic rotor speed

Degrees Of Freedom

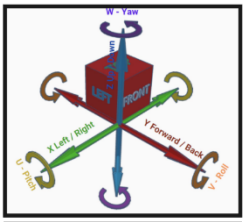

Fig.2 6 Degrees Of Freedom

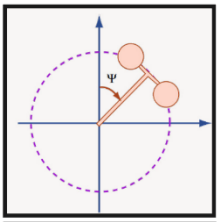

Fig.3., - Quanser Helicopter Travel Yaw.Angle (ψ)

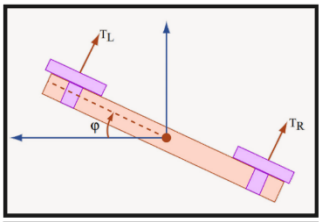

Fig.4., - Quanser Helicopter Roll (φ) Angle with Rotor Forces

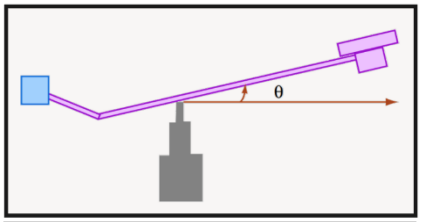

Fig.5., - Quanser Helicopter Pitch (θ) Angle with Support Stand

A free-flying-helicopter is characterised by six degrees of freedom, represented in Figure 1, whereas the Quanser Helicopter used in this project is restricted to three. These restrictions apply to roll, pitch and yaw, as shown in Figures 3, 4, and 5. In The helicopter's yaw movement is demonstrated across a fixed point, known as the vertical axis, as demonstrated in Figure 3. The trajectory of the helicopter's boom (the helicopter's arm that supports both rotors) is represented by the dashed line within the schematic, depending on the viewpoint of the helicopter. The notations of T_L and T_R in Figure 4, represent the left and the right rotors of the Quanser Helicopter. The schematic also shows how the rotors affect the roll of the system, allowing the helicopter to tilt left and right. The Quanser system is driven by two rotor speeds, with the inputs being V_{cyc} and V_{coll} The input V_{cyc} is an electrical voltage that induces a differential change in the speeds of the two rotors, while V_{coll} is an electrical voltage that controls the overall speeds of the propellers (Zenati, 2024). Figure 5 illustrates the helicopter's pitch angle, representing its tilt around the lateral axis. The pitch is regulated by V_{coll}, which adjusts the speeds of both rotors simultaneously, enabling the helicopter to rise or drop in altitude.

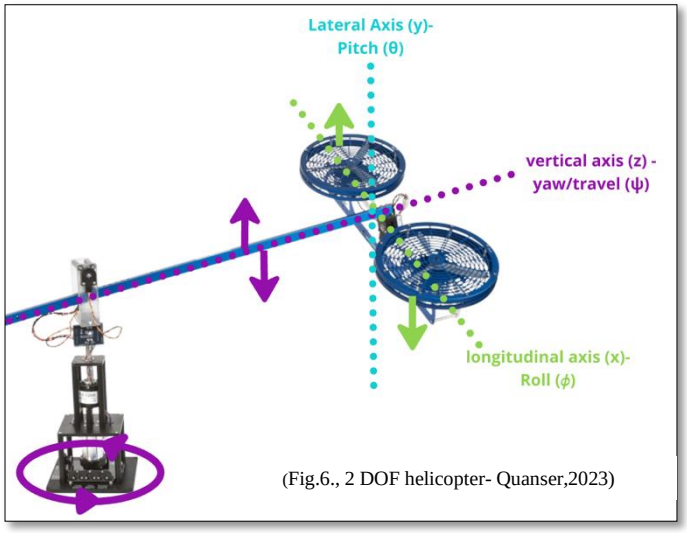

(Fig.6., 2 DOF helicopter- Quanser,2023)

Physical Parameters & Limits

Table [1] outlines the value limits that the Quanser helicopter must adhere to during the simulation. These limits are taken into consideration in the state-space computations.

Table [2] presents the geometric parameters, which likewise are to be used in state-space-computations.

Block Diagrams to explain pitch & roll

Voltage (V, Volts)	Roll Angle (ϕ)	Pitch Angle (θ)
$-5 \leq V \leq 5$	$-40^o \leq \phi \leq 40^o$	$-25^o \leq \theta \leq 25^o$

Table 1. Limit values for Quanser helicopter

Parameter	Value	Units
m	1.15	kg
M	3.57	kg
l_{boom}	0.66	m
l_ϕ	0.004	m
l_θ	0.014	m
l_h	0.177	m
I_{xx}	0.036	Nm

Parameter	Value	Units
I_{yy}	0.93	Nm
I_{zz}	0.036	Nm
K_τ	4.25e-3	N/s
θ_{rest}	-25	degs
g	9.81	m/s^2
L_p	[0.02,0.2]	
M_q	[0.1.0.9]	

Table 2. Geometric parameters

Block Diagrams for pitch and roll control system:

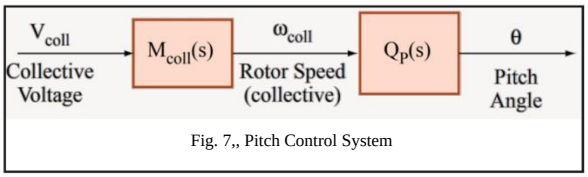

Fig. 7,, Pitch Control System

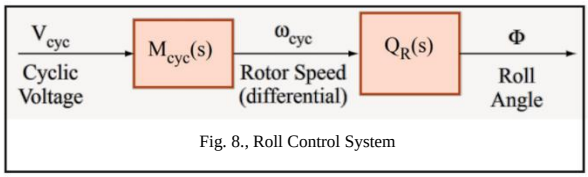

Fig. 8., Roll Control System

The block diagrams represent a simplified, linearised control model for the 'Quanser system', which focuses on both the pitch (θ) and roll (φ) subsystems. These block diagrams are characterized by the use of transfer functions, which are mathematical models that describe the linear time-invariant dynamics of a system. Transfer functions provide a compact representation of the relationship between the system's input and output (uk.mathworks.com, n.d.).

Figure 7 illustrates the pitch control of the Quanser helicopter with V_{coll} as the initial input. This system includes two transfer function blocks: $M_{coll}(s)$ and $Q_p(s)$, where both bocks represent the delay and gradual build-up for a set voltage/set rotor speed. $M_{coll}(s)$ converts V_{coll} into ω_{coll} and $Q_p(s)$ then transforms $\omega_{coll.}$ into a corresponding pitch angle (θ).

Figure 8 represents the roll control of the Quanser Helicopter with V_{cyc} as the initial input. Similar to the pitch control system, this system also includes two transfer function blocks: $M_{cyc}(s)$ and $Q_R(s)$. These two transfer blocks also account for the delay and gradual build-up associated with a given voltage or rotor speed. The block $M_{cyc}(s)$ converts V_{cyc} into ω_{cyc}, while $Q_R(s)$, transfers ω_{cyc} into a corresponding roll angle (φ).

Part 1:

Model Linearisation – State - Space - Representation

- Nonlinear equations of motion:

  [1] $I_{xx}\ddot{\phi} = \tau_{cyc}\, l_h - m\, g\, l_\theta \sin(\phi) - L_p\, \dot{\phi} - I_r\, \omega_{rotor}\, (\dot{\theta}\cos(\phi) + \dot{\psi}\sin(\phi))$

  [2] $I_{yy}\ddot{\theta} = \tau_{coll}\, l_{boom}\cos(\phi) - M\, g\, l_\theta \sin(\theta + \theta_{rest}) - D\, l_{boom}\sin(\gamma) + I_r\, \omega_{rotor}\, \dot{\phi} - M_q\dot{\theta}$

  [3] $I_{zz}\ddot{\psi} = \tau_{coll}\, l_{boom}\sin(\phi) - D\, l_{boom}\cos(\gamma)$

- Where:

  [4] $D = K_D\, \dot{\psi}$

  [5] $\tau_{coll} = K_\tau\, \omega_{coll} - K_v\, \dot{\psi}$

  [6] $\tau_{cyc} = K_\tau\, \omega_{cyc} - K_v\, \dot{\psi}$

- Motor dynamics modelling:

  [7] $\dot{\omega_{cyc}} + 6\, \omega_{cyc} = 780\, V_{cyc}$

  [8] $\dot{\omega_{coll}} + 6\, \omega_{coll} = 540\, V_{coll}$

- Steady-state hover conditions:

[A] $\dot{\psi}_0 = 0$ [B] $\dot{\phi}_0 = 0$ [C] $\dot{\theta}_0 = 0$ [D] $\psi_0 = 0$ [E] $\phi_0 = 0$ [F] $\theta_0 = 0$

[G] $\dot{\omega_{cyc,0}} = 0$ [H] $\dot{\omega_{coll,0}} = 0$ [I] $\gamma_0 = 0$ [J] $\omega_{rotor} = 0$

- State-space representation:

$$x_1 = \phi \quad x_2 = \dot{\phi} \quad x_3 = \theta \quad x_4 = \dot{\theta} \quad x_5 = \psi \quad x_6 = \dot{\psi}$$

$$x = \begin{bmatrix} x_1 = \phi \\ x_2 = \dot{\phi} \\ x_3 = \theta \\ x_4 = \dot{\theta} \\ x_5 = \psi \\ x_6 = \dot{\psi} \end{bmatrix} \qquad \dot{x} = \begin{bmatrix} \dot{x_1} = x_2 = \dot{\phi} \\ \dot{x_2} = \text{EQ [1a]} \\ \dot{x_3} = x_4 = \dot{\theta} \\ \dot{x_4} = \text{EQ [2a]} \\ \dot{x_5} = x_6 = \dot{\psi} \\ \dot{x_6} = \text{EQ [3a]} \end{bmatrix}$$

- **Re-arrange EQ [7] & EQ [8] for ω_{cyc} & ω_{coll}:**

EQ [7a]: $\frac{780\, V_{cyc} - \dot{\omega_{cyc}}}{6} = \omega_{cyc}$

EQ [8a]: $\frac{540\, V_{coll} - \dot{\omega_{coll}}}{6} = \omega_{coll}$

- **State-space representation of EQ [1] & re-arrange for $\ddot{\phi}$ ($\dot{x_2}$):**

$$\ddot{\phi} = \frac{1}{I_{xx}} [\tau_{cyc}\, l_h - m\, g\, l_\phi \sin(\phi) - L_p \dot{\phi} - I_r\, \omega_{rotor}\, (\dot{\theta}\cos(\phi) + \dot{\psi}\sin(\phi))]$$

- Sub in EQ [6]

$$\ddot{\phi} = \frac{1}{I_{xx}} [(K_\tau\, \omega_{cyc} - K_v \dot{\psi})\, l_h - m\, g l_\theta \sin(\phi) - L_p\, \dot{\phi} - I_r\, \omega_{rotor}\, (\dot{\theta}\cos(\phi) + \dot{\psi}\sin(\phi))]$$

- State-space representation:

$$\dot{x_2} = \frac{1}{I_{xx}} [(K_\tau\, \omega_{cyc} - K_v x_6)\, l_h - m\, g l_\theta \sin(x_1) - L_p\, x_2 - I_r\, \omega_{rotor}\, (x_4 \cos(x_1) + x_6 \sin(x_1))]$$

- Sub EQ [7a]

$$\dot{x_2} = \frac{1}{I_{xx}} [(K_\tau \frac{780\, V_{cyc} - \dot{\omega_{cyc}}}{6} - K_v x_6)\, l_h - m\, g l_\theta \sin(x_1) - L_p\, x_2 - I_r\, \omega_{rotor}\, (x_4 \cos(x_1) + x_6 \sin(x_1))]$$

Expand to give EQ [1a]

$$\dot{x_2} = \frac{1}{Ixx} [(130\, V_{cyc} K_\tau\, l_h - \frac{\dot{\omega_{cyc}}}{6} K_\tau\, l_h - K_v\, x_6 l_h - m\, g\, l_\theta \sin(x_1) - L_p\, x_2 - I_r\, \omega_{rotor}\, x_4 \cos(x_1) + I_r\, \omega_{rotor}\, x_6 \sin(x_1)]$$

- **State-space representation of EQ [2] & re-arrange for $\ddot{\theta}$ ($\dot{x_4}$)**

$$\ddot{\theta} = \frac{1}{I_{yy}} [\tau_{coll}\, l_{boom} \cos(\phi) - M\, g\, l_\theta \sin(\theta + \theta_{rest}) - D l_{boom} \sin(\gamma) + I_r\, \omega_{rotor}\, \dot{\phi}\, M_q \dot{\theta}]$$

- Sub EQ [5] & EQ [4]

$$\ddot{\theta} = \frac{1}{I_{yy}}[(K_\tau\,\omega_{coll} - K_v\,\dot{\psi})\,l_{boom}\cos(\phi) - M\,g\,l_\theta \sin(\theta + \theta_{rest}) - K_D\,\dot{\psi}\,l_{boom}\sin(\gamma) + I_r\,\omega_{rotor}\,\dot{\phi} - M_q\dot{\theta}]$$

- Expand via sin (a + b) = sin (a) cos (b) + cos (a) sin (b)

$$\ddot{\theta} = \frac{1}{I_{yy}}[(K_\tau\,\omega_{coll} - K_v\,\dot{\psi})\,l_{boom}\cos(\phi) - M\,g\,l_\theta(\sin(\theta)\cos(\theta_{rest}) + \cos(\theta)\sin(\theta_{rest})) - K_D\,\dot{\psi}\,l_{boom}\sin(\gamma) + I_r\,\omega_{rotor}\,\dot{\phi} - M_q\dot{\theta}]$$

- State-space representation:

$$\dot{x_4} = \frac{1}{I_{yy}}[(K_\tau\,\omega_{coll} - K_v\,x_6)\,l_{boom}\cos(x_1) - M\,g\,l_\theta\sin(x_3)\cos(\theta_{rest}) - M\,g\,l_\theta\cos(x_3)\sin(\theta_{rest}) - K_D\,x_6\,l_{boom}\sin(\gamma) + I_r\,\omega_{rotor}\,x_2 - M_q x_4]$$

- Sub EQ [8a]

$$\dot{x_4} = \frac{1}{I_{yy}}[(K_\tau\,\frac{540\,V_{coll} - \dot{\omega_{coll}}}{6} - K_v\,x_6)\,l_{boom}\cos(x_1) - M\,g\,l_\theta\sin(x_3)\cos(\theta_{rest}) - M\,g\,l_\theta\cos(x_3)\sin(\theta_{rest}) - K_D\,x_6\,l_{boom}\sin(\gamma) + I_r\,\omega_{rotor}\,x_2 - M_q x_4]$$

Expand to give EQ [2a]

$$\dot{x_4} = \frac{1}{I_{yy}}[90\,K_\tau\,V_{coll}\,l_{boom}\cos(x_1) - \frac{\dot{\omega_{coll}}}{6}K_\tau\,l_{boom}\cos(x_1) - K_v\,x_6\,l_{boom}\cos(x_1) - M\,g\,l_\theta\sin(x_3)\cos(\theta_{rest}) - M\,g\,l_\theta\cos(x_3)\sin(\theta_{rest}) - K_D\,x_6\,l_{boom}\sin(\gamma) + I_r\,\omega_{rotor}\,x_2 - M_q x_4]$$

- **State- space representation of EQ [3], re-arrange for $\ddot{\psi}$ ($\dot{x_6}$) & sub EQ [5]:**

$$\ddot{\psi} = \frac{1}{I_{zz}}[\tau_{coll}\,l_{boom}\sin(\phi) - D\,l_{boom}\cos(\gamma)]$$

- Sub EQ [4] & EQ [5]

$$\ddot{\psi} = \frac{1}{I_{zz}}[(K_\tau\,\omega_{coll} - K_v\,\dot{\psi})\,l_{boom}\sin(\phi) - (K_D\,\dot{\psi})\,l_{boom}\cos(\gamma)]$$

- State-space representation:

$$\dot{x_6} = \frac{1}{I_{zz}}[(K_\tau\,\omega_{coll} - K_v\,x_6)\,l_{boom}\sin(x_1) - (K_D\,x_6)\,l_{boom}\cos(\gamma)]$$

- Sub EQ [8a]

$$\dot{x_6} = \frac{1}{I_{zz}}[(K_\tau\,\frac{540\,V_{coll} - \dot{\omega_{coll}}}{6} - K_v\,x_6)\,l_{boom}\sin(x_1) - (K_D\,x_6)\,l_{boom}\cos(\gamma)]$$

Expand to give EQ [3a]

$$\dot{x_6} = \frac{1}{I_{zz}}[(90\,K_\tau V_{coll}\,l_{boom}\sin(x_1) - \frac{\dot{\omega_{coll}}}{6}K_\tau l_{boom}\sin(x_1) - K_v\,x_6\,l_{boom}\sin(x_1) - (K_D\,x_6)\,l_{boom}\cos(\gamma)]$$

- **Apply partial differentials w.r.t to states, to satisfy steady state:**

$\dot{\mathbf{x}} = \mathbf{Ax} + \mathbf{Bu}$ state equation

$\mathbf{y} = \mathbf{Cx} + \mathbf{Du}$ output equation

for $t \geq t_0$ and initial conditions, $\mathbf{x}(t_0)$, where

$\mathbf{x}$ = state vector
$\dot{\mathbf{x}}$ = derivative of the state vector with respect to time
$\mathbf{y}$ = output vector
$\mathbf{u}$ = input or control vector
$\mathbf{A}$ = system matrix
$\mathbf{B}$ = input matrix
$\mathbf{C}$ = output matrix
$\mathbf{D}$ = feedforward matrix

Figure 9. Steady State Governing equations

The state equation and output equation will describe the dynamics of the Quanser helicopter in terms of roll, pitch, and yaw. To obtain the state and output equations shown in Figure 1, the state-space representations of roll, pitch, and yaw derived thus far must be linearized, as these equations contain nonlinear terms.

Therefore, to form the A, B, C, and D matrices, partial derivatives with respect to the states must be applied to linearise the equations, as illustrated in Figure 10. Additionally, steady-state conditions, as defined by equations [A] to [J], and small-angle approximations must be applied.

$$\hat{\mathbf{A}} = \left.\frac{\partial \mathbf{f}}{\partial \mathbf{x}}\right|_{(\mathbf{x}_e,\mathbf{u}_e)} \triangleq \left[\begin{matrix} \frac{\partial f_1}{\partial x_1} & \frac{\partial f_1}{\partial x_2} & \cdots & \frac{\partial f_1}{\partial x_n} \\ \frac{\partial f_2}{\partial x_1} & \frac{\partial f_2}{\partial x_2} & \cdots & \frac{\partial f_2}{\partial x_n} \\ \vdots & \vdots & \vdots & \vdots \\ \frac{\partial f_n}{\partial x_1} & \frac{\partial f_n}{\partial x_2} & \cdots & \frac{\partial f_n}{\partial x_n} \end{matrix}\right]_{(\mathbf{x}_e,\mathbf{u}_e)}, \quad \hat{\mathbf{B}} = \left.\frac{\partial \mathbf{f}}{\partial \mathbf{u}}\right|_{(\mathbf{x}_e,\mathbf{u}_e)} \triangleq \left[\begin{matrix} \frac{\partial f_1}{\partial u_1} & \frac{\partial f_1}{\partial u_2} & \cdots & \frac{\partial f_1}{\partial u_m} \\ \frac{\partial f_2}{\partial u_1} & \frac{\partial f_2}{\partial u_2} & \cdots & \frac{\partial f_2}{\partial u_m} \\ \vdots & \vdots & \vdots & \vdots \\ \frac{\partial f_n}{\partial u_1} & \frac{\partial f_n}{\partial u_2} & \cdots & \frac{\partial f_n}{\partial u_m} \end{matrix}\right]_{(\mathbf{x}_e,\mathbf{u}_e)}$$

$$\hat{\mathbf{C}} = \left.\frac{\partial \mathbf{h}}{\partial \mathbf{x}}\right|_{(\mathbf{x}_e,\mathbf{u}_e)} \triangleq \left[\begin{matrix} \frac{\partial h_1}{\partial x_1} & \frac{\partial h_1}{\partial x_2} & \cdots & \frac{\partial h_1}{\partial x_n} \\ \frac{\partial h_2}{\partial x_1} & \frac{\partial h_2}{\partial x_2} & \cdots & \frac{\partial h_2}{\partial x_n} \\ \vdots & \vdots & \vdots & \vdots \\ \frac{\partial h_p}{\partial x_1} & \frac{\partial h_p}{\partial x_2} & \cdots & \frac{\partial h_p}{\partial x_n} \end{matrix}\right]_{(\mathbf{x}_e,\mathbf{u}_e)}, \quad \hat{\mathbf{D}} = \left.\frac{\partial \mathbf{h}}{\partial \mathbf{u}}\right|_{(\mathbf{x}_e,\mathbf{u}_e)} \triangleq \left[\begin{matrix} \frac{\partial h_1}{\partial u_1} & \frac{\partial h_1}{\partial u_2} & \cdots & \frac{\partial h_1}{\partial u_m} \\ \frac{\partial h_2}{\partial u_1} & \frac{\partial h_2}{\partial u_2} & \cdots & \frac{\partial h_2}{\partial u_m} \\ \vdots & \vdots & \vdots & \vdots \\ \frac{\partial h_p}{\partial u_1} & \frac{\partial h_p}{\partial u_2} & \cdots & \frac{\partial h_p}{\partial u_m} \end{matrix}\right]_{(\mathbf{x}_e,\mathbf{u}_e)}$$

Figure 10: A B C D matrix equations

*Note:
$\delta f_n - n$ *repersents the row of the matrix*
$\delta x_z - z$ *repersents the corresponding state in analysis*
Cos ≈ 1
Sin ≈ 0
$x_1, x_2, x_3, x_4, x_5, x_6, \dot{\omega}_{coll}, \dot{\omega}_{cyc}, \omega_{rotor} \approx 0$

$$f_n = \begin{bmatrix} \dot{x_1} = f_1 \\ \dot{x_2} = \text{EQ [1a]} = f_2 \\ \dot{x_3} = f_3 = \\ \dot{x_4} = \text{EQ [2a]} = f_4 \\ \dot{x_5} = f_5 \\ \dot{x_6} = \text{EQ [3a]} = f_6 \end{bmatrix} \qquad h_n = \begin{bmatrix} x_1 \\ x_3 \\ x_5 \end{bmatrix}$$

Calculating $\widehat{A}$ matrix:

1. $\frac{\delta f_1}{\delta x_n}$ **:**

$f_1 = x_2$

$\frac{\delta f_1}{\delta x_1} \equiv \frac{\delta f_1}{\delta x_3} \equiv \frac{\delta f_1}{\delta x_4} \equiv \frac{\delta f_1}{\delta x_5} \equiv \frac{\delta f_1}{\delta x_6} \equiv 0$

$\frac{\delta f_1}{\delta x_2} = 1$

2. $\frac{\delta f_2}{\delta x_n}$ **:**

$f_2 = \frac{1}{\text{Ixx}} [130\, V_{cyc} \text{K}_\tau\, l_h - \frac{\dot{\omega}_{cyc}}{6} \text{K}_\tau\, l_h - \text{K}_v\, x_6 l_h - \text{m g}\, l_\theta \sin(x_1) - \text{L}_p\, x_2 - \text{I}_r\, \omega_{\text{rotor}}\, x_4 \cos(x_1) + \text{I}_r\, \omega_{\text{rotor}}\, x_6 \sin(x_1)]$

$\frac{\delta f_2}{\delta x_3} = \frac{\delta f_2}{\delta x_5} = 0$

$\frac{\delta f_2}{\delta x_1} = (\frac{1}{\text{Ixx}} [- \text{m g l}_\theta \cos(x_1) + \text{I}_r\, \omega_{\text{rotor}}\, x_4 \sin(x_1) - \text{I}_r\, \omega_{\text{rotor}}\, x_6 \cos(x_1)])$

Apply steady-state conditions: $= \frac{- \text{m g l}_\theta \cos(x_1)}{\text{I}_{xx}}$

Apply small angle approx. → $\frac{\delta f_2}{\delta x_1} = - \frac{\text{m g l}_\theta}{\text{I}_{xx}}$

$\frac{\delta f_2}{\delta x_2} = (\frac{1}{\text{I}_{xx}} [- \text{L}_p\,]) = - \frac{L_p}{\text{I}_{xx}}$

$\frac{\delta f_2}{\delta x_4} = (\frac{1}{\text{I}_{xx}} [\ - \text{I}_r\, \omega_{\text{rotor}} \cos(x_1)\ ])$

Apply small angle approx. & steady state → $\frac{\delta f_2}{\delta x_4} = 0$

$\frac{\delta f_2}{\delta x_6} = \frac{1}{\text{Ixx}} [- \text{Kv}\, l_h + \text{I}_r\, \omega_{\text{rotor}} \sin(x_1)]$

$= \frac{- \text{K}_v\, \text{l}_h + \text{I}_r\, \omega_{rotor} \sin(x_1)}{\text{I}_{xx}}$

Apply small angle approx. & steady state → $\frac{\delta f_2}{\delta x_6} = - \frac{\text{K}_v\, \text{l}_h}{\text{I}_{xx}}$

3. $\frac{\delta f_3}{\delta x_n}$ **:**

$f_3 = x_4$

$\frac{\delta f_3}{\delta x_1} \equiv \frac{\delta f_3}{\delta x_2} \equiv \frac{\delta f_3}{\delta x_3} \equiv \frac{\delta f_3}{\delta x_5} \equiv \frac{\delta f_3}{\delta x_6} \equiv 0$

$\frac{\delta f_3}{\delta x_4} = 1$

4. $\frac{\delta f_4}{\delta x_n}$ **:**

$f_4 = \frac{1}{I_{yy}}$ [90 K_τ $V_{coll} l_{boom} \cos(x_1)$ – $\frac{\dot{\omega}_{coll}}{6}$ K_τ $l_{boom} \cos(x_1)$ – K_v x_6 $l_{boom} \cos(x_1)$ – M g l_θ $\sin(x_3) \cos(\theta_{rest})$ – M g l_θ $\cos(x_3) \sin(\theta_{rest})$ – K_D x_6 $l_{boom} \sin(\gamma)$ + I_r ω_{rotor} x_2 –$M_q x_4$]

$\frac{\delta f_4}{\delta x_1} = \frac{1}{I_{yy}}$ [-90 K_τ $V_{coll} l_{boom} \sin(x_1)$ + $\frac{\dot{\omega}_{coll}}{6}$ K_τ $l_{boom} \sin(x_1)$ + K_v x_6 $l_{boom} \sin(x_1)$]

$= \frac{1}{I_{yy}}$ [-90 K_τ $V_{coll} l_{boom} \sin(x_1)$ + $\frac{\dot{\omega}_{coll}}{6}$ K_τ $l_{boom} \sin(x_1)$]

Apply small angle approx. & steady-state→ $\frac{\delta f_4}{\delta x_1} = 0$

$\frac{\delta f_4}{\delta x_2} = \frac{1}{I_{yy}}$ [I_r ω_{rotor}] = $\frac{I_r \omega_{rotor}}{I_{yy}}$

Apply steady-state condition→ $\frac{\delta f_4}{\delta x_2} = 0$

$\frac{\delta f_4}{\delta x_3} = \frac{1}{I_{yy}}$ [– M g l_θ $\cos(x_3) \cos(\theta_{rest})$ + M g l_θ $\sin(x_3) \sin(\theta_{rest})$]

Apply small angle approx. → $\frac{\delta f_4}{\delta x_3} = -\frac{M g l_\theta \cos(\theta_{rest})}{I_{yy}}$

$\frac{\delta f_4}{\delta x_4} = \frac{1}{I_{yy}}$ [$-M_q$] = $-\frac{M_q}{I_{yy}}$

$\frac{\delta f_4}{\delta x_5} = 0$

$\frac{\delta f_4}{\delta x_6} = -K_v$ $l_{boom} \cos(x_1) – K_D$ $l_{boom} \sin(\gamma)$

Apply small angle approx. → $\frac{\delta f_4}{\delta x_6} = 0$

5. $\frac{\delta f_5}{\delta x_n}$ **:**

$f_5 = x_6$

$\frac{\delta f_5}{\delta x_1} \equiv \frac{\delta f_5}{\delta x_2} \equiv \frac{\delta f_5}{\delta x_3} \equiv \frac{\delta f_5}{\delta x_4} \equiv \frac{\delta f_5}{\delta x_5} \equiv 0$

$\frac{\delta f_5}{\delta x_6} = 1$

6. $\frac{\delta f_6}{\delta x_n}$ **:**

$f_6 = \frac{1}{I_{zz}}[\,(90\ K_\tau V_{coll} l_{boom} \sin(x_1) - \frac{\dot{\omega}_{coll}}{6} K_\tau\, l_{boom} \sin(x_1) - K_v\, x_6\, l_{boom} \sin(x_1) - (K_D\ x_6)\ l_{boom} \cos(\gamma)]$

$\frac{\delta f_6}{\delta x_2} \equiv \frac{\delta f_6}{\delta x_3} \equiv \frac{\delta f_6}{\delta x_4} \equiv \frac{\delta f_6}{\delta x_5} \equiv 0$

$\frac{\delta f_6}{\delta x_1} = \frac{1}{I_{zz}}[90\ K_\tau V_{coll} l_{boom} \cos(x_1) - \frac{\dot{\omega}_{coll}}{6} K_\tau\, l_{boom} \cos(x_1) - K_v\, x_6\, l_{boom} \cos(x_1)]$

Apply small angle approx. & steady-state $\rightarrow \frac{\delta f_6}{\delta x_1} = \frac{90\ K_\tau\, V_{coll}\, l_{boom}}{I_{zz}}$

$\frac{\delta f_6}{\delta x_6} = \frac{1}{I_{zz}}[-K_v\ l_{boom} \sin(x_1) - K_D\, l_{boom} \cos(\gamma)]$

Apply small angle approx. & steady-state $\rightarrow \frac{\delta f_6}{\delta x_6} = \frac{-K_D\ l_{boom}}{I_{zz}}$

Therefore, Matrix $\widehat{A}$ is:

$$\widehat{A} = \begin{bmatrix} 0 & 1 & 0 & 0 & 0 & 0 \\ -\frac{m\, g\, l_\theta}{I_{xx}} & -\frac{l_p}{Ixx} & 0 & 0 & 0 & -\frac{K_v\, l_h}{I_{xx}} \\ 0 & 0 & 0 & 1 & 0 & 0 \\ 0 & 0 & -\frac{M\, g\, l_\theta \cos(\theta_{rest})}{I_{yy}} & -\frac{M_q}{I_{yy}} & 0 & 0 \\ 0 & 0 & 0 & 0 & 0 & 1 \\ \frac{90\ K_\tau\, V_{coll}\, l_{boom}}{I_{zz}} & 0 & 0 & 0 & 0 & \frac{-K_D\ l_{boom}}{I_{zz}} \end{bmatrix}$$

Calculating $\widehat{B}$ matrix:

U=[V_{cyc} V_{coll}] where, $U_1 = V_{cyc}$ & $U_2 = V_{coll}$

1. $\frac{\delta f_1}{\delta U_n}$ **:**

$f_1 = x_2$

$\frac{\delta f_1}{\delta U_1} = 0$

$\frac{\delta f_1}{\delta U_2} = 0$

2. $\frac{\delta f_2}{\delta U_n}$ **:**

$f_2 = \frac{1}{I_{xx}}$ [130 V_{cyc} K_τ l_h − $\frac{\dot{\omega}_{cyc}}{6}$ K_τ l_h − K_v $x_6 l_h$ − m g l_θ sin (x_1) − L_p x_2 −I_r ω_{rotor} x_4 cos (x_1) + I_r ω_{rotor} x_6 sin (x_1)]

$\frac{\delta f_2}{\delta U_1} = \frac{130\ K_\tau\ l_h}{I_{xx}}$

$\frac{\delta f_2}{\delta U_2} = 0$

3. $\frac{\delta f_3}{\delta U_n}$ **:**

$f_3 = x_4$

$\frac{\delta f_3}{\delta U_1} = 0$

$\frac{\delta f_3}{\delta U_2} = 0$

4. $\frac{\delta f_4}{\delta U_n}$ **:**

$f_4 = \frac{1}{I_{yy}}$ [90 K_τ $V_{coll} l_{boom}$ cos(x_1) − $\frac{\dot{\omega}_{coll}}{6}$ K_τ l_{boom} cos(x_1) − K_v x_6 l_{boom} cos(x_1) − M g l_θ sin (x_3) cos (θ_{rest}) − M g l_θ cos (x_3) sin (θ_{rest}) − K_D x_6 l_{boom} sin(γ) + I_r ω_{rotor} x_2 −$M_q x_4$]

$\frac{\delta f_4}{\delta U_1} = 0$

$\frac{\delta f_4}{\delta U_2} = \frac{90\ K_\tau\ l_{boom}}{I_{yy}}$

5. $\frac{\delta f_5}{\delta U_n}$ **:**

$f_5 = x_6$

$\frac{\delta f_5}{\delta U_1} = 0$

$\frac{\delta f_5}{\delta U_2} = 0$

6. $\frac{\delta f_6}{\delta U_n}$ **:**

$f_6 = \frac{1}{I_{zz}}$ [(90 $K_\tau V_{coll} l_{boom} \sin(x_1)$ $- \frac{\dot{\omega_{coll}}}{6} K_\tau\, l_{boom} \sin(x_1) - K_v\, x_6\, l_{boom} \sin(x_1)$ $-$ (K_D x_6) $l_{boom} \cos(\gamma)$]

$\frac{\delta f_6}{\delta U_1} = 0$

$\frac{\delta f_6}{\delta U_2} = 0$

Therefore, Matrix $\widehat{B}$ is:

$$\widehat{B} = \begin{bmatrix} 0 & 0 \\ \frac{130\ K_\tau\ l_h}{I_{xx}} & 0 \\ 0 & 0 \\ 0 & \frac{90\ K_\tau\ l_{boom}}{I_{yy}} \\ 0 & 0 \\ 0 & 0 \end{bmatrix}$$

Calculating $\widehat{C}$ matrix:

$y = h(x, u)$

$$y = \begin{bmatrix} \phi \\ 0 \\ \theta \\ 0 \\ \psi \\ 0 \end{bmatrix} = \begin{bmatrix} x_1 \\ 0 \\ x_3 \\ 0 \\ x_5 \\ 0 \end{bmatrix} \begin{matrix} \leftarrow h_1 \\ \leftarrow h_2 \\ \leftarrow h_3 \\ \leftarrow h_4 \\ \leftarrow h_5 \\ \leftarrow h_6 \end{matrix}$$

1. $\frac{\delta h_1}{\delta x_n}$ **:**

$\frac{\delta h_1}{\delta x_1} = 1$

$\frac{\delta h_1}{\delta x_2} = \frac{\delta h_1}{\delta x_3} = \frac{\delta h_1}{\delta x_4} = \frac{\delta h_1}{\delta x_5} = \frac{\delta h_1}{\delta x_6} = 0$

2. $\frac{\delta h_2}{\delta x_n}$ **:**

$\frac{\delta h_2}{\delta x_1} = \frac{\delta h_2}{\delta x_2} = \frac{\delta h_2}{\delta x_3} = \frac{\delta h_2}{\delta x_4} = \frac{\delta h_2}{\delta x_5} = \frac{\delta h_2}{\delta x_6} = 0$

3. $\frac{\delta h_3}{\delta x_n}$ **:**

$$\frac{\delta h_3}{\delta x_3} = 1$$

$$\frac{\delta h_3}{\delta x_1} = \frac{\delta h_3}{\delta x_2} = \frac{\delta h_3}{\delta x_4} = \frac{\delta h_3}{\delta x_5} = \frac{\delta h_3}{\delta x_6} = 0$$

4. $\frac{\delta h_4}{\delta x_n}$ **:**

$$\frac{\delta h_4}{\delta x_1} = \frac{\delta h_4}{\delta x_2} = \frac{\delta h_4}{\delta x_3} = \frac{\delta h_4}{\delta x_4} = \frac{\delta h_4}{\delta x_5} = \frac{\delta h_4}{\delta x_6} = 0$$

5. $\frac{\delta h_5}{\delta x_n}$ **:**

$$\frac{\delta h_5}{\delta x_5} = 1$$

$$\frac{\delta h_5}{\delta x_1} = \frac{\delta h_5}{\delta x_2} = \frac{\delta h_5}{\delta x_3} = \frac{\delta h_5}{\delta x_4} = \frac{\delta h_5}{\delta x_6} = 0$$

6. $\frac{\delta h_6}{\delta x_n}$ **:**

$$\frac{\delta h_6}{\delta x_1} = \frac{\delta h_6}{\delta x_2} = \frac{\delta h_6}{\delta x_3} = \frac{\delta h_6}{\delta x_4} = \frac{\delta h_6}{\delta x_5} = \frac{\delta h_6}{\delta x_6} = 0$$

Therefore, Matrix $\widehat{C}$ is:

$$\hat{C} = \begin{bmatrix} 1 & 0 & 0 & 0 & 0 & 0 \\ 0 & 0 & 0 & 0 & 0 & 0 \\ 0 & 0 & 1 & 0 & 0 & 0 \\ 0 & 0 & 0 & 0 & 0 & 0 \\ 0 & 0 & 0 & 0 & 1 & 0 \\ 0 & 0 & 0 & 0 & 0 & 0 \end{bmatrix}$$

Calculating $\widehat{D}$ matrix:

$$y = \begin{bmatrix} \phi \\ 0 \\ \theta \\ 0 \\ \psi \\ 0 \end{bmatrix} = \begin{bmatrix} x_1 \\ 0 \\ x_3 \\ 0 \\ x_5 \\ 0 \end{bmatrix} \begin{matrix} \leftarrow h_1 \\ \leftarrow h_2 \\ \leftarrow h_3 \\ \leftarrow h_4 \\ \leftarrow h_5 \\ \leftarrow h_6 \end{matrix}$$

$\widehat{D} = \frac{\delta h_n}{\delta x_n} = 0$ → *as no U terms in output equation 'y'*

Full state equation →$\dot{x} = Ax + Bu$:

$$\begin{bmatrix} \dot{x_1} \\ \dot{x_2} \\ \dot{x_3} \\ \dot{x_4} \\ \dot{x_5} \\ \dot{x_6} \end{bmatrix} = \begin{bmatrix} 0 & 1 & 0 & 0 & 0 & 0 \\ -\frac{m\, g\, l_\theta}{I_{xx}} & -\frac{l_p}{Ixx} & 0 & 0 & 0 & -\frac{K_v\, l_h}{I_{xx}} \\ 0 & 0 & 0 & 1 & 0 & 0 \\ 0 & 0 & -\frac{M\, g\, l_\theta \cos(\theta_{rest})}{I_{yy}} & -\frac{M_q}{I_{yy}} & 0 & 0 \\ 0 & 0 & 0 & 0 & 0 & 1 \\ \frac{90\, K_\tau\, V_{coll}\, l_{boom}}{I_{zz}} & 0 & 0 & 0 & 0 & \frac{-K_D\, l_{boom}}{I_{zz}} \end{bmatrix} \begin{bmatrix} x_1 \\ x_2 \\ x_3 \\ x_4 \\ x_5 \\ x_6 \end{bmatrix} + \begin{bmatrix} 0 & 0 \\ \frac{130\, K_\tau\, l_h}{I_{xx}} & 0 \\ 0 & 0 \\ 0 & \frac{90\, K_\tau\, l_{boom}}{I_{yy}} \\ 0 & 0 \\ 0 & 0 \end{bmatrix} [V_{cyc} \quad V_{coll}]$$

Full output equation →$y = Cx + Du$:

$$\begin{bmatrix} x_1 \\ 0 \\ x_3 \\ 0 \\ x_5 \\ 0 \end{bmatrix} = \begin{bmatrix} 1 & 0 & 0 & 0 & 0 & 0 \\ 0 & 0 & 0 & 0 & 0 & 0 \\ 0 & 0 & 1 & 0 & 0 & 0 \\ 0 & 0 & 0 & 0 & 0 & 0 \\ 0 & 0 & 0 & 0 & 1 & 0 \\ 0 & 0 & 0 & 0 & 0 & 0 \end{bmatrix} \begin{bmatrix} x_1 \\ x_2 \\ x_3 \\ x_4 \\ x_5 \\ x_6 \end{bmatrix} + 0$$

Transfer Functions– [Part 1]

Below transfer functions for the following are derived:

[1] $M_{coll}(s)$: Via. Fig [6] & EQ [8]

EQ [8]: $\dot{\omega_{coll}} + 6\, \omega_{coll} = 540\, V_{coll}$

Fig [6] – Transfer Function = $M_{coll}(s) = \frac{\omega_{coll}(s)}{V_{coll}(s)}$

Represent via Laplace

$s\, \omega_{coll}(s) + 6\, \omega_{coll}(s) = 540\, V_{coll}(s)$

$(s+6)\, \omega_{coll}(s) = 540\, V_{coll}(s)$

Therefore

$$M_{coll}(s) = \frac{\omega_{coll}(s)}{V_{coll}(s)} = \frac{540}{s+6}$$

[2] $M_{cyc}(s)$: Via. Fig [7] & EQ [7]

EQ [7]: $\dot{\omega_{cyc}} + 6\ \omega_{cyc} = 780\ V_{cyc}$

Fig [6] – Transfer Function = $M_{cyc}(s) = \frac{\omega_{cyc}(s)}{V_{cyc}(s)}$

Represent via Laplace

$s\ \omega_{cyc}(s) + 6\ \omega_{cyc}(s) = 780\ V_{cyc}(s)$

$(s+6)\ \omega_{cyc}(s) = 780\ V_{cyc}(s)$

Therefore

$$M_{cyc}(s) = \frac{\omega_{cyc}(s)}{V_{cyc}(s)} = \frac{780}{s+6}$$

[3] $Q_P(s)$:

Figure 6, represents how $Q_P(s)$ relates to ω_{coll} & θ

EQ [2] : $I_{yy}\ddot{\theta} = \tau_{coll}\ l_{boom}\cos(\phi) - M\ g\ l_\theta \sin(\theta + \theta_{rest}) - D\ l_{boom}\sin(\gamma) + I_r\ \omega_{rotor}\ \dot{\phi} - M_q\dot{\theta}$

Apply small angle approximations:

$\cos(\phi) \approx 1 \qquad \sin(\theta) \approx \theta \qquad \sin(\gamma) \approx \gamma$

$I_{yy}\ddot{\theta} = \tau_{coll}\ l_{boom} - M\ g\ l_\theta\ (\theta + \theta_{rest}) - D\ l_{boom}\ \gamma + I_r\ \omega_{rotor}\ \dot{\phi} - M_q\dot{\theta}$

Substituting $\gamma_0 = 0$ & $\omega_{rotor} = 0$, gives:

$I_{yy}\ddot{\theta} = \tau_{coll}\ l_{boom} - M\ g\ l_\theta\ (\theta + \theta_{rest}) - M_q\dot{\theta}$

Laplacian Transform:

$I_{yy}\ s^2\ \theta(s) = \tau_{coll}\ l_{boom} - M\ g\ l_\theta\ \theta(s) + M\ g\ l_\theta\ \theta_{rest} - M_q\ s\ \theta(s)$

Re-arrange for all 's' terms on LHS:

$I_{yy}\ s^2\ \theta(s) + M_q\ s\ \theta(s) + M\ g\ l_\theta\ \theta(s) = \tau_{coll}\ l_{boom} + M\ g\ l_\theta\ \theta_{rest}$

Sub in for τ_{coll} (EQ [5]):

$I_{yy}\ s^2\ \theta(s) + M_q\ s\ \theta(s) + M\ g\ l_\theta\ \theta(s) = (K_\tau\ \omega_{coll} - K_v\ \dot{\psi})\ l_{boom} + M\ g\ l_\theta\ \theta_{rest}$

Substituting $\dot{\psi}_0 = 0$ gives:

$I_{yy}\ s^2\ \theta(s) + M_q\ s\ \theta(s) + M\ g\ l_\theta\ \theta(s) = K_\tau\ \omega_{coll}\ l_{boom} + M\ g\ l_\theta\ \theta_{rest}$

"$Q_P(s)$ relates to ω_{coll} & θ", via Fig.6:

$\theta(s)\ [I_{yy}\ s^2 + M_q\ s + M\ g\ l_\theta] = K_\tau\ \omega_{coll}\ l_{boom} + M\ g\ l_\theta\ \theta_{rest}$

$M\ g\ l_\theta\ \theta_{rest}$ can be neglected since, it is a steady-state bias; therefore, the following only focuses on the dynamic behaviour:

$\theta(s)\ [I_{yy}\ s^2 + M_q\ s + M\ g\ l_\theta] = K_\tau\ \omega_{coll}\ l_{boom}$

Therefore, the transfer function of $Q_p(s)$:

$$\frac{\theta(s)}{\omega_{coll}} = \frac{K_\tau\ l_{boom}}{I_{yy}\ s^2 + M_q\ s + M\ g\ l_\theta} = Q_p(s)$$

[4] $Q_R(s)$:

Via Fig.6, presents how $Q_R(s)$ relates to ω_{cyc} & ϕ
EQ [1]: $I_{xx}\ddot{\phi} = \tau_{cyc} l_h - m\ g\ l_\theta \sin(\phi) - L_p\dot{\phi} - I_r\omega_{rotor}(\dot{\theta}\cos(\phi) + \dot{\psi}\sin(\phi))$

Apply small angle approximations & steady state conditions:
$\cos(\phi) \approx 1$ $\sin(\theta) \approx \theta$ $\sin(\gamma) \approx \gamma$
$\dot{\psi}_0 = 0$ $\gamma_0 = 0$ $\omega_{rotor} = 0$

$I_{xx}\ddot{\phi} = \tau_{cyc} l_h - m\ g\ l_\theta \phi - L_p\dot{\phi}$

Sub EQ [6]:
$I_{xx}\ddot{\phi} = (K_\tau\omega_{cyc} - K_v\dot{\psi}) l_h - m\ g\ l_\theta \phi - L_p\dot{\phi}$

Re-apply steady state:
$I_{xx}\ddot{\phi} = K_\tau\omega_{cyc} l_h - m\ g\ l_\theta \phi - L_p\dot{\phi}$

Re-arrange $\ddot{\phi}$ & apply Laplace:
$\ddot{\phi} = \frac{1}{I_{xx}}[= K_\tau\omega_{cyc} l_h - m\ g\ l_\theta \phi - L_p\dot{\phi}]$

$s^2\phi(s) = \frac{1}{I_{xx}}[K_\tau\omega_{cyc} l_h - m\ g\ l_\theta \phi(s) - L_p\ s\ \phi(s)]$

$\phi(s)[s^2 + \frac{m\ g\ l_\theta}{I_{xx}} + \frac{L_p\ s}{I_{xx}}] = \frac{K_\tau\omega_{cyc} l_h}{I_{xx}}$

Therefore, $Q_r(s)$ is the following:
$\frac{\phi(s)}{\omega_{cyc}} = \frac{K_\tau\ l_h}{I_{xx}\ s^2 + m\ g\ l_\theta + L_p\ s]} = Q_r(s)$

Controller for roll (ϕ) and pitch (θ):

The following section details the design of a roll and pitch control using classical design techniques, ensuring that the following properties are met:

- Less than 10% error in tracking signals with frequency content up to 1 rad/s
- At least 20° of phase margin
- Maintain stability even in worst-case damping

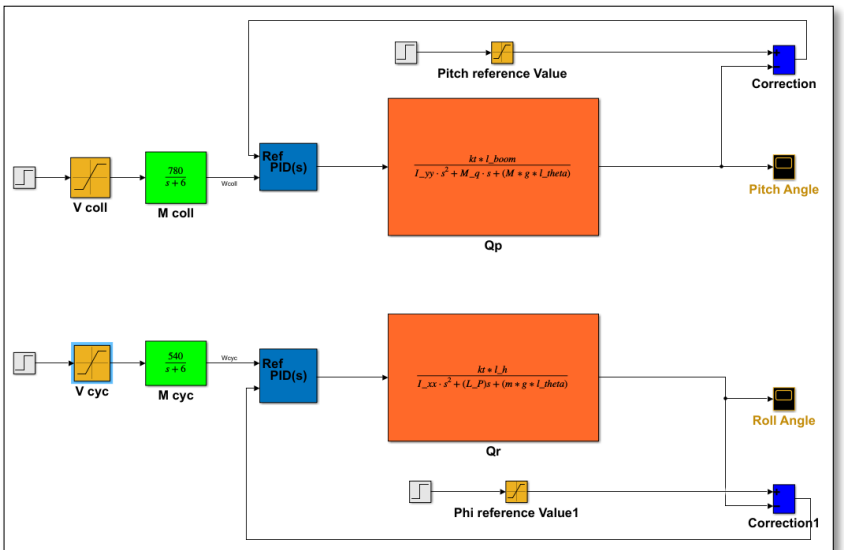

Figure 11: Pitch and Roll Controller Design using a PID Controller on Simulink

Design Strategy:

Decoupling Pitch and Roll Control

Pitch and roll are treated independently in the design to reduce system complexity. This decoupling simplifies the tuning process for each axis, allowing for more precise adjustments without interference from the other axis. By handling pitch and roll separately, each control loop can be optimised independently, improving overall system performance.

PID control

Tasked with designing a controller using classical design techniques, the implementation of a PID controller seemed natural. PID control is a simple and effective method, widely used in aerospace applications for stability control (Ogata, 2010) (Nise, 2011). By adjusting the proportional, integral, and derivative gains, the PID controller can fine-tune the system's response to minimize tracking errors and maintain stability (Astrom, Hagglund, 2006). The 3 terms the PID autotunes is the proportional, integral and derivative term. The proportional gain is tuned to reduce rise time and steady state error but can lead to overshoot (Umich.edu, 2023). Derivative control tends to reduce the overshoot generated by the proportional control and the settling time. Finally, the integral gain reduces the rise tine and steady state error. After several iterations of tuning PID control, the proportional, integral and derivative gains shall provide the desired response (Umich.edu, 2023).

Additionally, the PID controller is self-tuning, automatically adjusting its parameters based on the error signal, ensuring stability even under varying conditions (Gawthrop, Smith, 2011) Mehmet, Yılmaz, 2016). The use of independent PID control loops for pitch and roll allows each axis to be regulated separately, eliminating any cross-coupling effects (Liu, Wang,2014).

Damping Conditions

Damping significantly affects system response. To ensure robustness, the controller was tested across a range of damping coefficients, as outlined in the flowchart (Figure X), confirming stable performance under various damping scenarios.

Real-Time Feedback Loop

The design incorporates a continuous real-time feedback loop that compares the actual pitch and roll angles with the desired values. This loop continuously adjusts the system to minimize tracking errors, ensuring precise and stable performance.

Performance Verification

Performance was verified using error tracking graphs and Bode plots. Tracking error graphs confirm the controller maintains errors below 10%, while Bode plots validate stability and robustness under dynamic conditions.

Implementation in MATLAB/Simulink

The control algorithms were implemented in MATLAB and Simulink for real-time simulation and PID tuning. This platform allows for rapid adjustments based on system response, ensuring optimal controller performance.

Block diagram:

This block diagram represents a control system for managing the pitch and roll angles of a Quanser helicopter using PID controllers.

Pitch Controller:

1. **Input:** V_{coll}, which is an electrical voltage that controls the overall speeds of the propellers.
2. **$M_{coll}(s)$ transfer function:** models the dynamics of the system between voltage input and resulting angular velocity.
3. **PID controller:** adjust the collective rotor speed to minimise the error between the desired pitch angle and the actual pitch angle. Ensures precise and stable pitch tracking by dynamically adjusting the system's response. Here the proportional gain has been tuned to 12, the integral gain to 0.035 and the derivative gain to 1.2, filter coefficient (N) to 150, setpoint weight b to 0.02 and setpoint weight c to 0.1. This was achieved by trial and error, with initial auto tuning.
4. **$Q_p(s)$ transfer function:** represents physical dynamics of helicopter pitch angle.
5. **Output & correction:** system outputs the actual pitch angle and compares with reference angle. A correction signal is generated to refine the input V_{coll} via the feedback loop.

Roll Controller:

1. **Input:** V_{cyc}, which is an electrical voltage that induces a differential change in the speeds of the two.
2. **$M_{cyc}(s)$ transfer function** models the dynamics of the system between voltage input and resulting angular velocity.
3. **PID controller:** adjust the cyclic rotor speed to minimize the error between the desired roll angle and the actual roll angle. Ensures precise and stable roll tracking by dynamically adjusting the system's response. Here the proportional gain has been tuned to 0.5, the integral gain to 0.004, derivative gain to 0.1, filter coefficient (N) to 100 ,setpoint weight b to 3 and setpoint weight c to 0.5. This was achieved by trial and error, with initial auto tuning.
4. **$Q_p(s)$ transfer function** represents physical dynamics of helicopter roll angle.
5. **Output & correction:** system outputs the actual roll angle and compares with reference. A correction signal is generated to refine the input V_{cyc} via the feedback loop.

Predicted performance:

Stability: As Pitch and roll has been decoupled, the PID controller should provide good stability as since each axis is treated independently it allows more targeted optimisation of PID parameters to each desired angle.

Responsiveness: Again, with both pitch and roll being treated independently and the subsequent optimal PID tuning to achieve desired response in both pitch and roll means quick response times and minimal overshoot is expected. This is crucial, as excessive overshoot in pitch or roll angles could potentially lead to stall conditions. While this may be less of a concern in a lab setting, in real-world applications, reaching a stall angle could have damaging effects.

Accuracy: Roll and pitch control is typically associated with small perturbations in angles hence the behaviour can be taken as linear (hence the linearisation for steady state conditions in the governing equation of motion). PID controllers are accurate for linear control hence its expected to work well in this specific application. The error tracking and real-time feedback

loop will ensure the roll angles stay close to the desired values minimising the error to less than 10%.

Robustness: Tuning the PID controller to account for the full range in damping conditions (both minimum and maximum conditions that the Quanser Helicopter may encounter) should ensure that the system is robust and can effectively handle disturbances and changes in load without significant performance degradation.

Verification of performance:

To ensure the controller meets the three specified properties and the predicted performance, several graphs were generated for verification. To confirm tracking performance has a less than 10% error, a step input tracking error graph is computed, as shown in Figure 20 snd 21. Robustness, defined by maintaining a phase margin of at least 20°, is verified using the Bode plots in Figure 24 and 25 with the subsequent phase margin annotated. Finally, stability under worst-case damping conditions is demonstrated by testing the controller across a range of low damping scenarios. This is illustrated by the Nyquist plots in Figure 22 and 23. A Matlab script is used to loop through values of L_p (roll damping coefficient and M_q (pitch damping coefficient) and plot this on the bode plots. A flow chart demonstrating the logic behind this code is shown in Figure X.

[1] Bode plot of the controller:

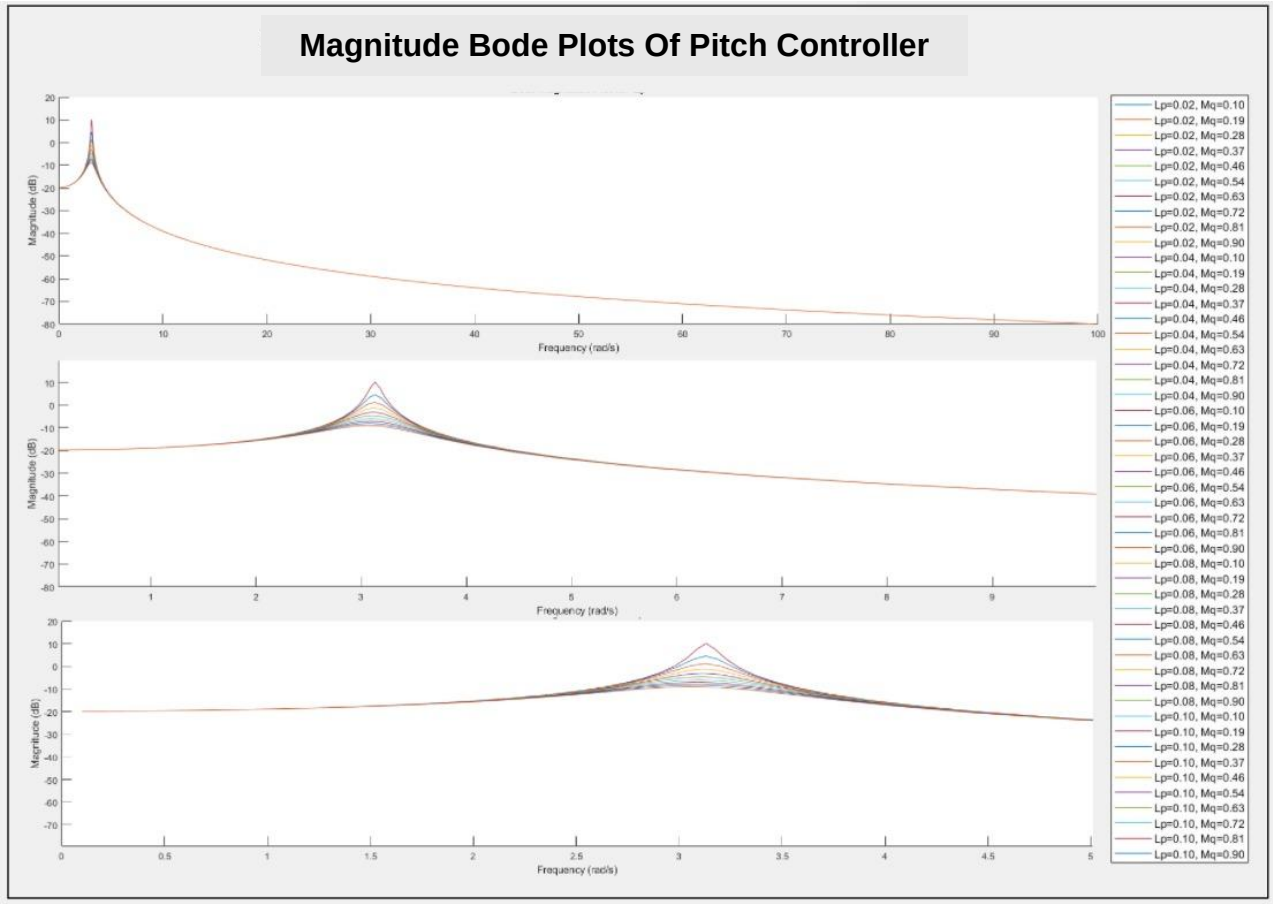

Figure 12. V_{coll} Controller Bode Plot Magnitude at varying L_P & M_q

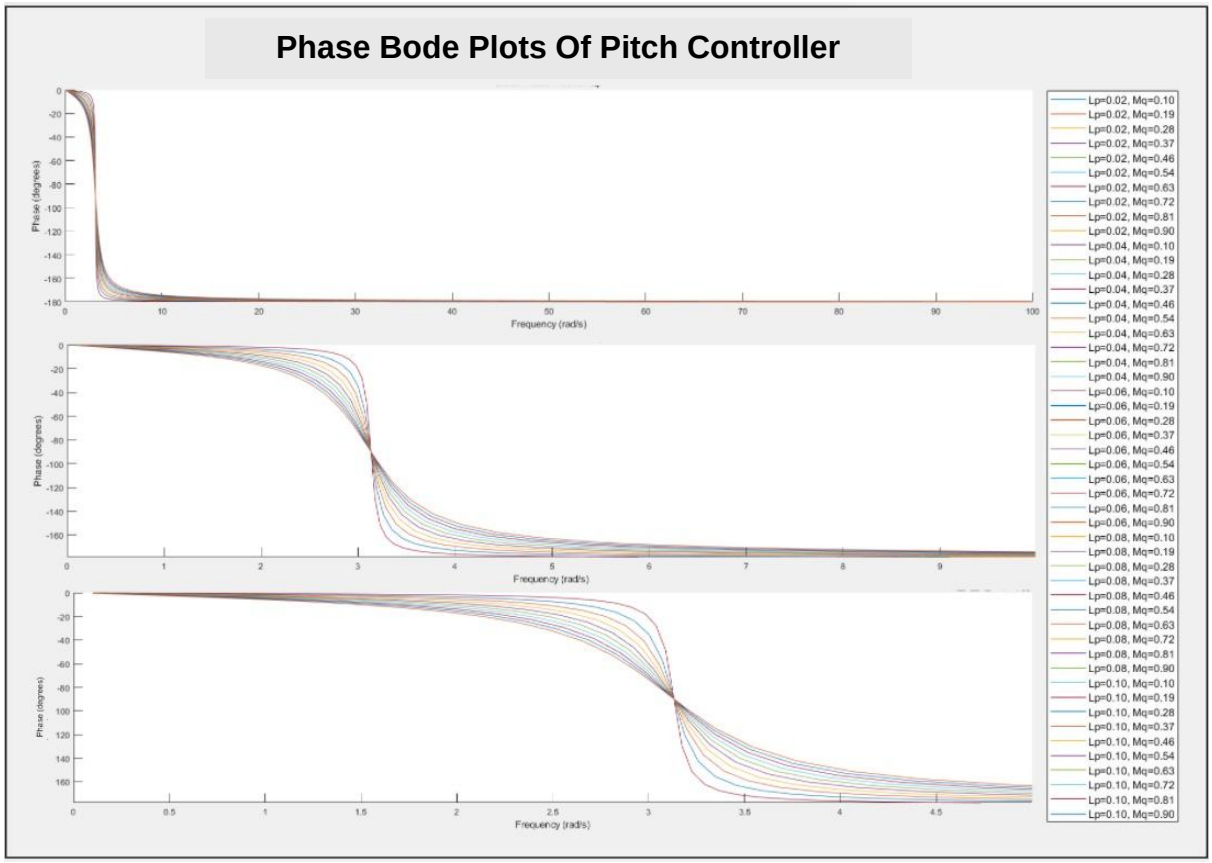

Figure 13. V_{coll} Controller Bode Plot phase at varying L_P & M_q

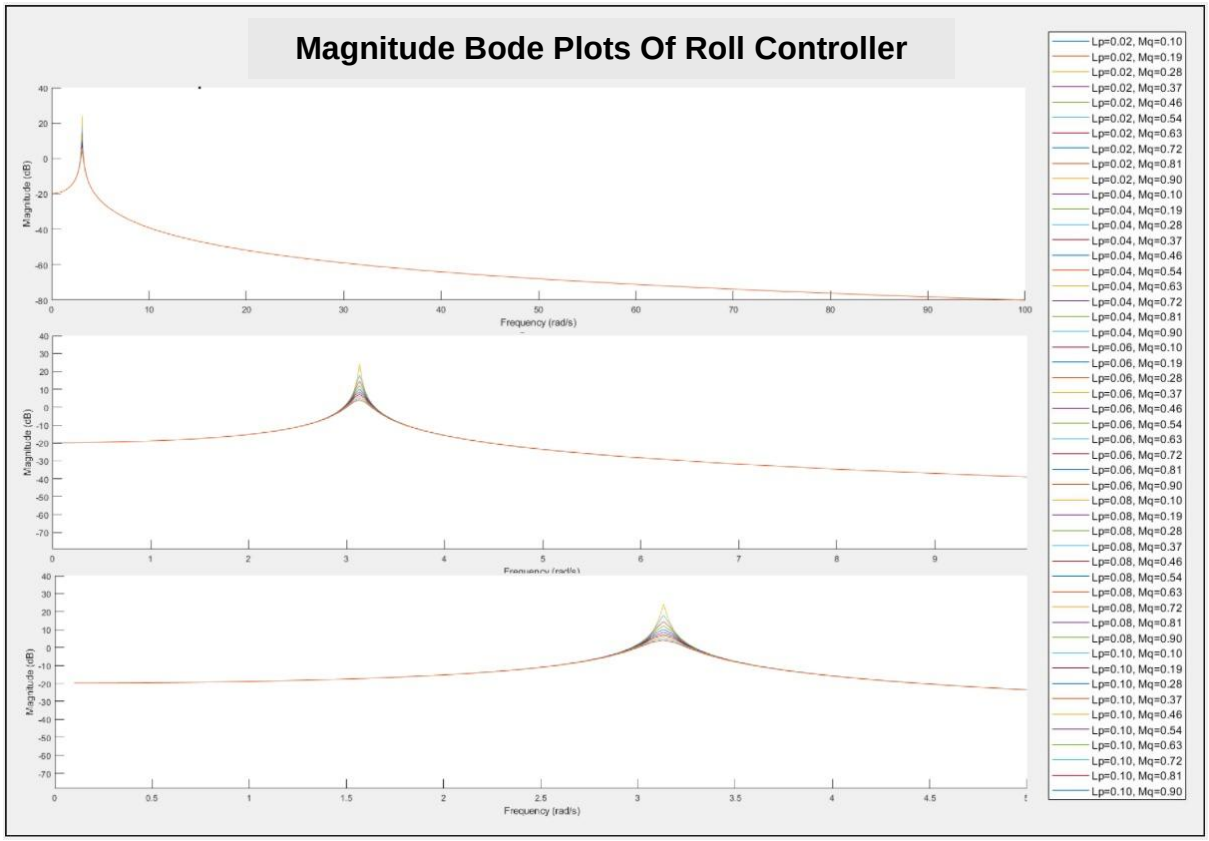

Figure 14. V_{cyc} Controller Bode Plot magnitude at varying L_P & M_q

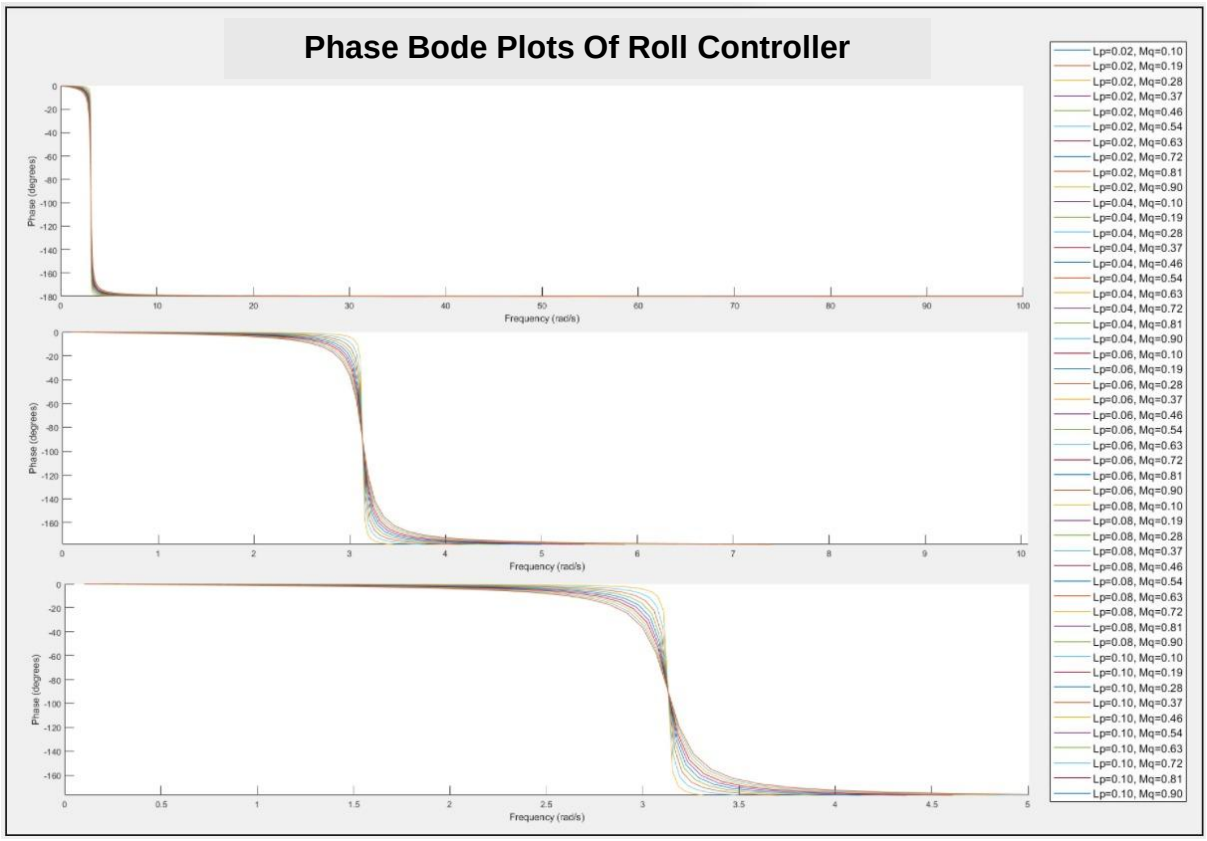

Figure 15. V_{coll} Controller Bode Plot magnitude at varying L_P & M_q

[2] Open loop Bode plot of controller + nominal plant:

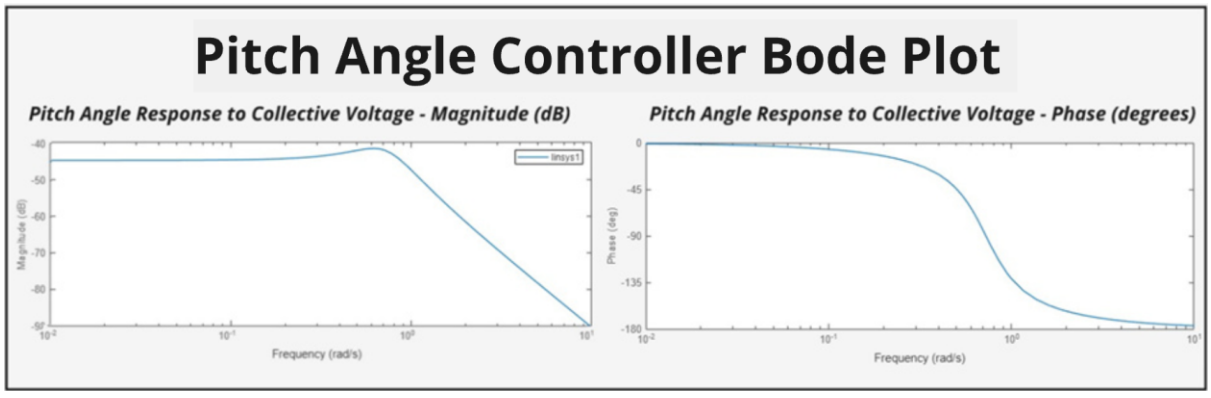

Figure 16. V_{coll} Controller Bode Plot at Nominal L_P & M_q

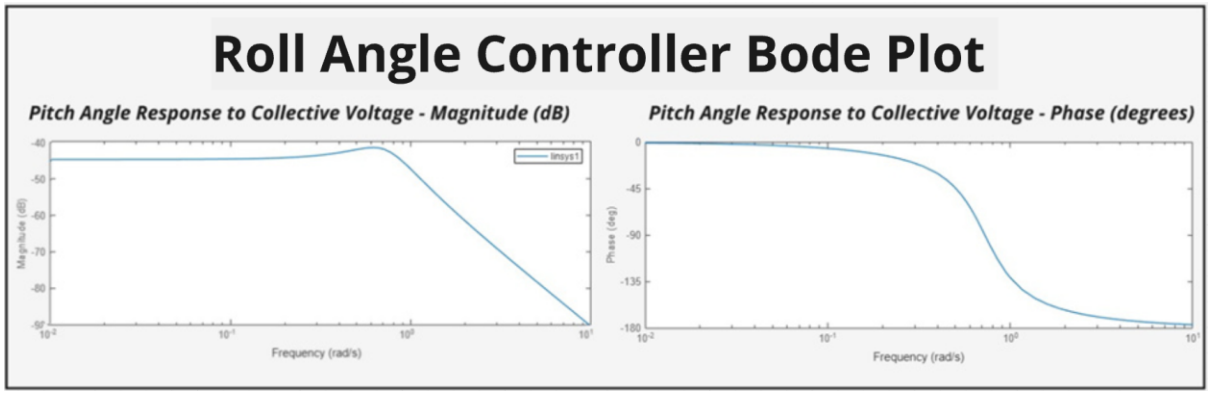

Figure 17. V_{cyc} Controller Bode Plot at Nominal LP & M

[3] Simulated closed-loop step response for a 20° step command:

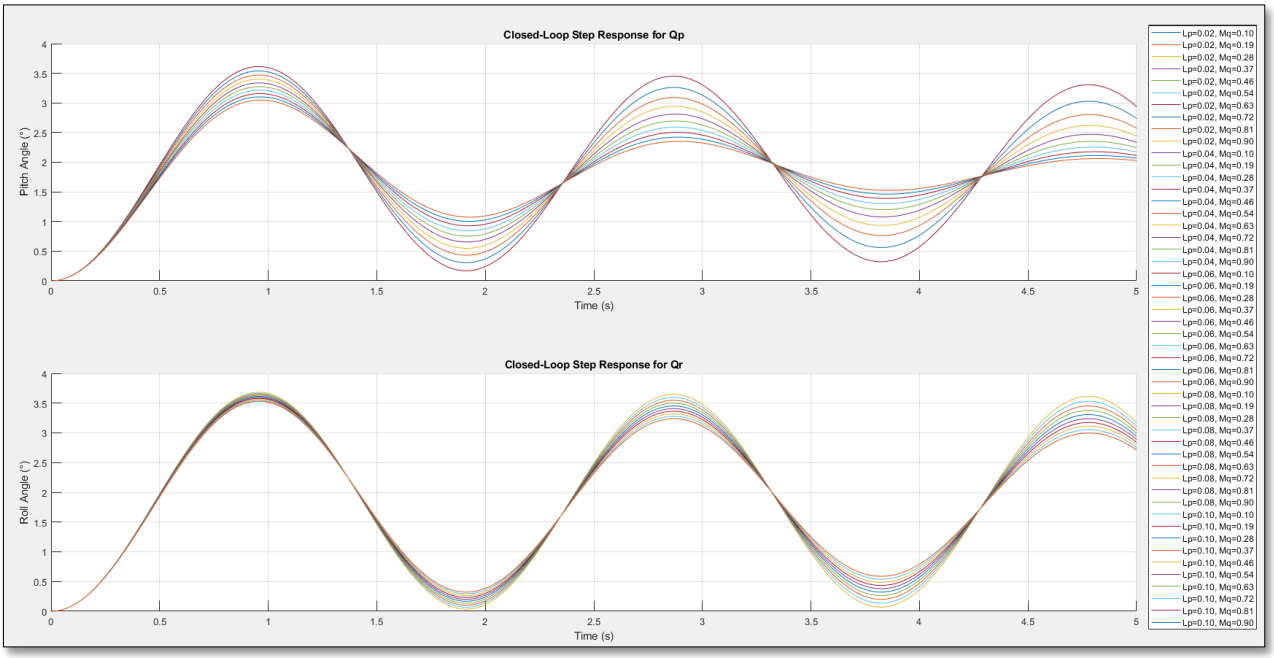

Figure 18. V_{coll} and V_{cyc} Controllers step response at 20ºPitch and Roll Controllers step response at 20º

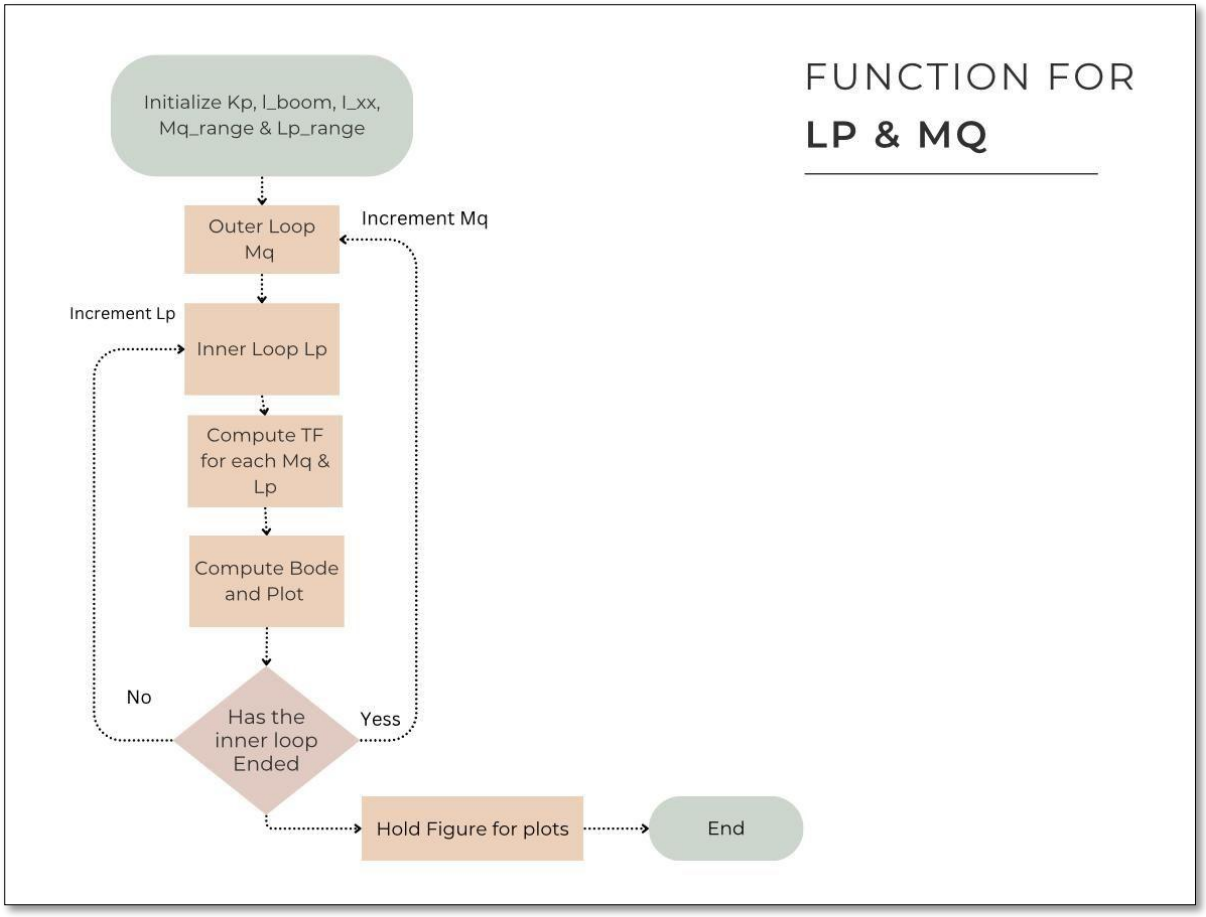

Figure 19. Lp & M_Q Looping Function

Performance:

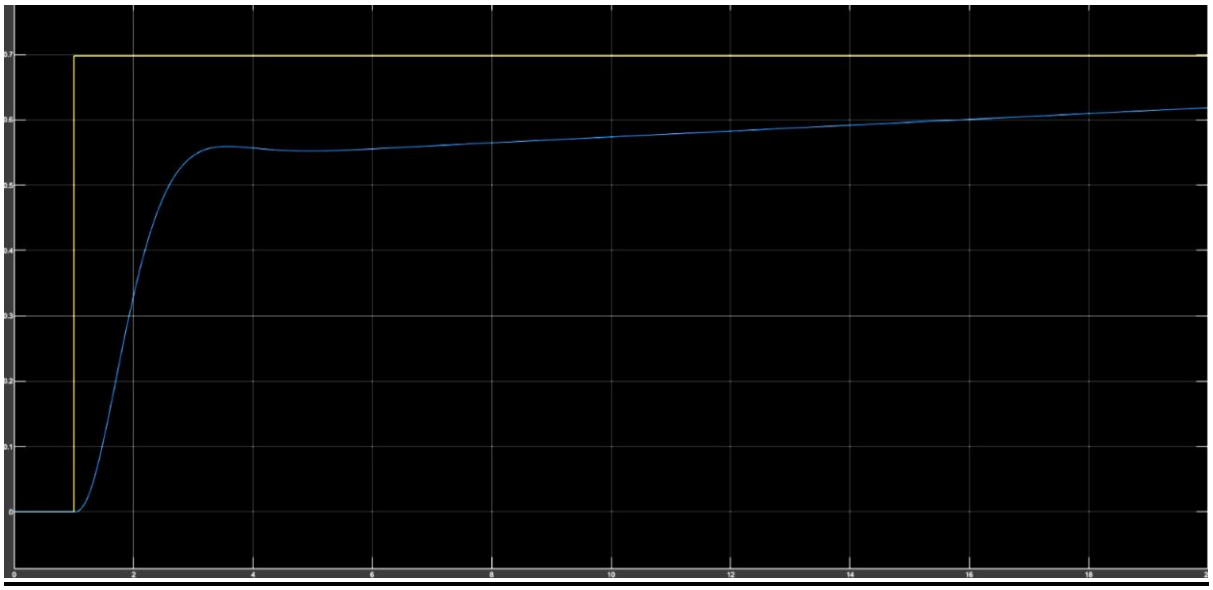

Figure 20. Error tracking graph for roll controller

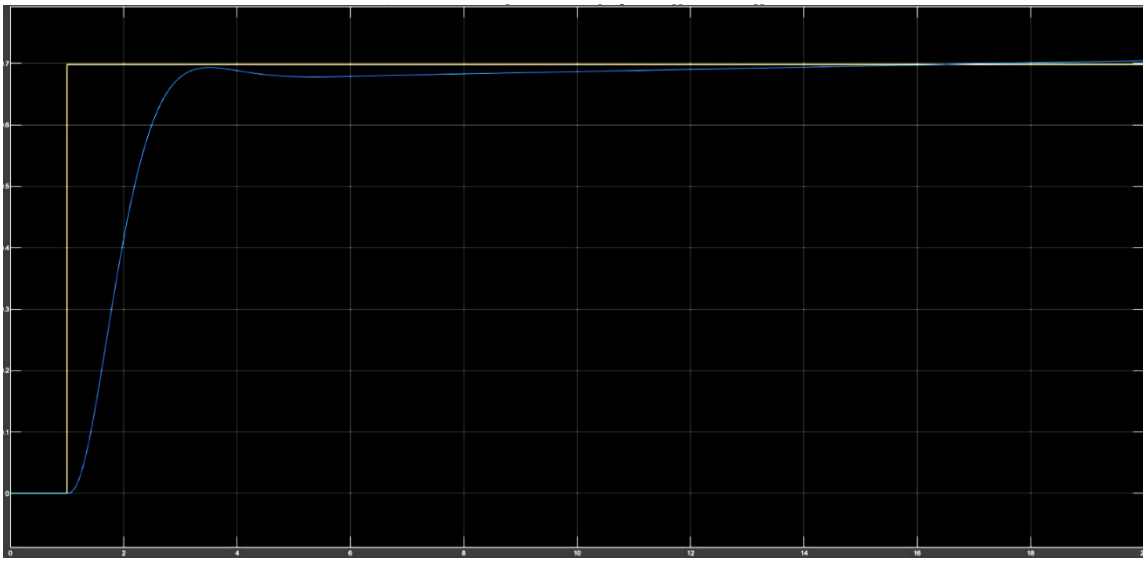

Figure 21. Error tracking graph for pitch controller

Figure 20 and 21, shows the output signal for both pitch and roll converge towards the desired value of 1 defined by the step input. Here we have fed a step input into the controller as the desired signal output. In Figure 20, the roll controller output is depicted, here we can see that roll angle effectively converges to the desired output with not only a quick response time of 0.6 seconds but with no overshoots. This performance demonstrates several strengths of the controller, including a tracking error of less than 10%. Specifically, for a frequency of 1 rad/s, the tracking error is just 0.6%, falling 94% below the target tracking limit. The absence of overshoot further enhances robustness, ensuring system stability without introducing oscillations or transient instabilities. In Figure 21, the pitch controller output is shown. Here we can see that again the pitch angle effectively converges to the desired output with response time of approximately 7.5 seconds. Similarly, to the roll controller at frequency of 1 rad/s, the tracking error is just 0.6%, falling 94% below the target tracking limit. While this response is slower than that of the roll controller, it is still relatively fast and well-suited for the application. The pitch controller exhibits a small overshoot during the transient response, measuring only 0.02 units above the desired magnitude. This minor overshoot does not pose a risk of reaching stall conditions or compromising system performance.

Both controllers demonstrate effective robustness and the ability to achieve quick responses, ensuring reliable performance under their respective conditions. While the roll controller offers a faster response with no overshoot, the pitch controller also performs admirably with a controlled overshoot and reasonable response time. Collectively, these results highlight the controllers' capability to handle dynamic scenarios with precision and stability.

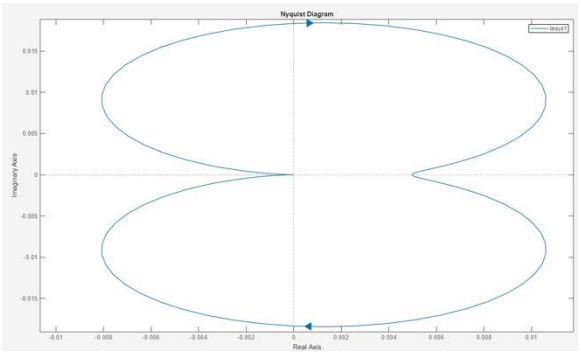

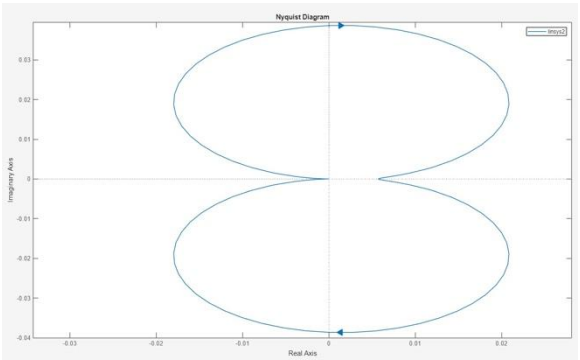

Figure 22. Nyquist Plot for roll controller

Figure 23. Nyquist Plot for pitch controller

Figure 22 and 23 are Nyquist plots, these show the stability of the systems under the full range of damping conditions. Nyquist criterion is determined by the absence of encirclement of $-1 + j0$. From both the plots we can see that Nyquist curve does not encircle $-1 + j0$ indicating the system is indeed stable even for worst case damping. Additionally, the fact that both plots appear to maintain a sufficient margin to $-1 + j0$ suggest sufficient robustness against potential variations or uncertainties in system parameters. This robustness implies that the system can tolerate changes or disturbances without crossing into instability, making it reliable for a wide range of operational conditions.

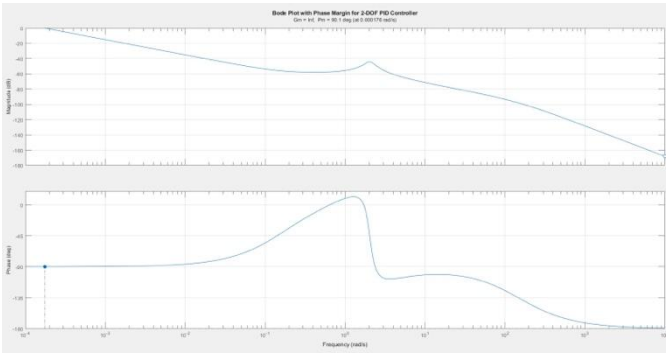

Figure 24. Bode plots of roll controller showing phase margin

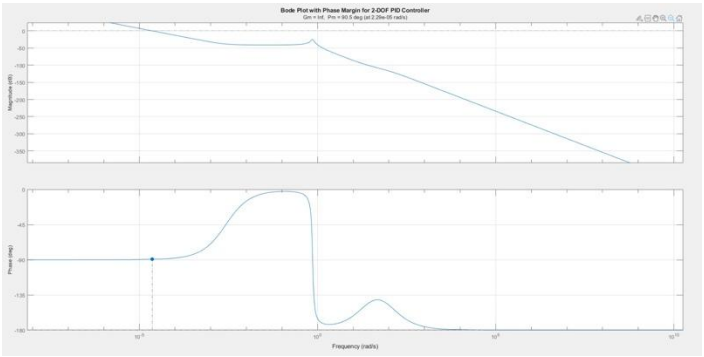

Figure 25. Bode plots of pitch controller showing phase margin

Figure 24 and Figure 25 show the phase margins of both the pitch and roll controllers. Both controllers achieve a phase margin of 90 degrees. A phase margin of 90 degrees typically indicates a stable system with minimal overshoot.

Ultimately, both roll and pitch controls meet the project's performance criteria and predicted outcomes, successfully maintaining control over the pitch and roll axes of the Quanser Helicopter.

Advantages of design	**Disadvantages of design**
Decoupled control for pitch and roll • Simplifies tuning process • Ensures more precise control for each axis	Decoupled control for pitch and roll • In reality pitch and roll axis will have an effect on one another. Decoupling reduces the realism of the model and may not fully capture the cross-coupling effects that occur in actual flight conditions.
Simplicity • PID controller is straightforward and widely recognised	Reactive control rather than predictive: • System responds to current errors without anticipating future behaviour. This can result in slower response times during dynamic behaviour

Real-time error minimisation: • Continuous feedback loop ensures errors are quickly detected and minimised allowing accurate tracking of desired pitch and roll angles	PID assumes linear behaviour • Doesn’t perform well in nonlinear environments such as rapid manoeuvres or large disturbances.

Part 2:

[2.1] Augmented plant Controller design for the Quanser Helicopter's ψ (Psi) Axis:

The term 'augmented' refers to the enhancement or expansion of a system's capabilities, in regard to it’s system dynamics. In this context, the two controllers for roll and pitch developed on the previous task, are to be augmented via incorporating Ψ (PSI) into their design considerations, rather than being limited to pitch and phi.

This integration will effectively embed the controllers to mimic a more realistic resulting behaviour. Below presents the Simulink environment for a controller taking Psi into consideration:

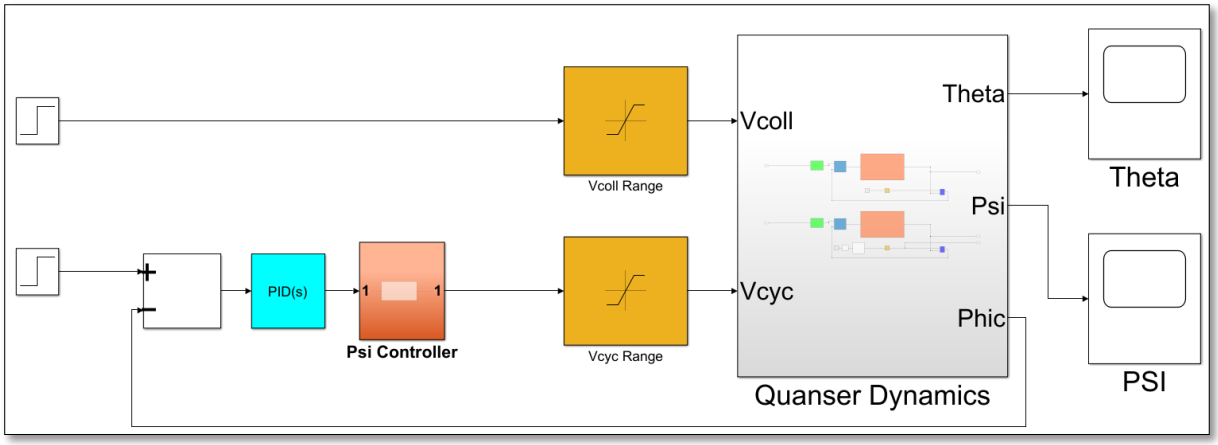

Figure 1 Psi Incorporated Controller Main hub

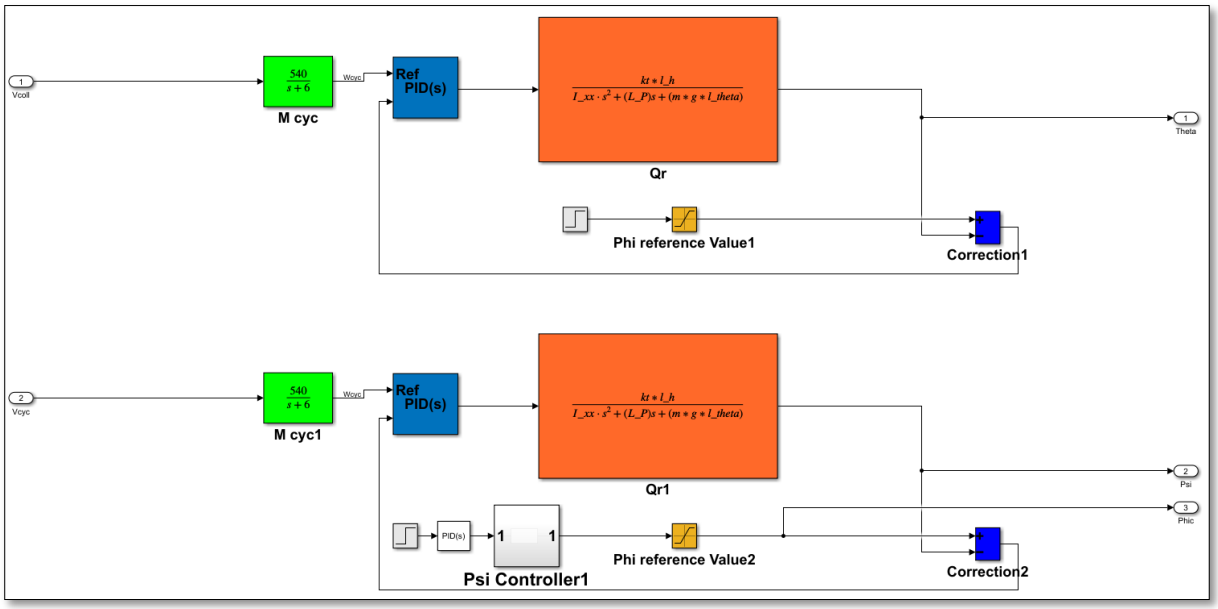

Figure 2 Quanser Dynamics Sub-System

To understand Fig.1. and Fig.2., one must initially understand the difference in controllers from part 1 and this part.

Previously designed, consisted of a theta and Phi system regulator based on simply using a 'saturated block', which takes both an upper and lower limit allowing for range. In addition, to this consisted of a step block, which allowed the range to be incremented as an iteration, with steps of one. This system here is then augmented to take Psi into consideration.
Via EQ [1], [2], [3], it is clear Psi and Phi are both independent of theta, hence, its noticeable in fig.2 the Psi controller is interconnected with Phi only.

The following formulas, define how the following controller operates:

[9] $V_{coll} = G_c^{pitch}(s)\,(\theta_c - \theta)$

[10] $V_{cyc} = G_c^{roll}(s)\,(\phi_c - \phi)$

[11] $\phi_c = G_c^{travel}(s)\ (\Psi_c - \Psi)$

[12] $G^{travel}(s) = \frac{\Psi(S)}{\phi_c(s)}$

EQ [9] & [10], demonstrates the governing pitch and roll equations, which in Fig.2 are presented by 2 "inner loops". Via closing these 2 inner loops, enables the controller to determine the true dynamics, presented in EQ [12], which has an input ϕ_c $(commanded\ roll\ angle)$ & corresponding output Ψ (travel angle).

The following data, in addition to Tables [1] & [2], have been provided, as following

Parameter	Value	Units	Description
I_{zz}	0.93	Nm	*Moment of inertia about the z-axis*
K_D	0		*Travel rate drag coefficient*
$\overline{\boldsymbol{\omega}}_{\boldsymbol{coll}}$	$\frac{Mgl_\theta \sin(\theta_{rest})}{K_T l_{boom}}$	N	*Trim collective thrust*
K_v	$0.0125\ \overline{\boldsymbol{\omega}}_{coll}\ K_T l_{boom}$		*Travel rate thrust coefficient*

-Psi Transfer Function Computation:

Sub EQ [4] & EQ [5] into EQ [3]

[3] $I_{zz}\ \ddot{\psi} = \tau_{coll}\ l_{boom} \sin(\phi) - D\ l_{boom} \cos(\gamma)$
[4] $D = K_D\ \dot{\psi}$
[5] $\tau_{coll} = K_\tau\ \omega_{coll} - K_v\ \dot{\psi}$

$I_{zz}\ \ddot{\psi} = (K_\tau\ \omega_{coll} - K_v\ \dot{\psi})\ l_{boom} \sin(\phi) - (K_D\ \dot{\psi})\ l_{boom} \cos(\gamma)$

Preform Expansion:
$I_{zz}\ \ddot{\psi} = K_\tau\ \omega_{coll}\ l_{boom} \sin(\phi) - K_v\ \dot{\psi}\ l_{boom} \sin(\phi) - K_D\ \dot{\psi}\ l_{boom} \cos(\gamma)$

Sub revised EQ[8]:
[8] $\dot{\omega_{coll}} + 6\ \omega_{coll} = 540\ V_{coll}$
Revised [8] $\frac{540V_{coll} - \dot{\boldsymbol{\omega}}_{\boldsymbol{coll}}}{6} = \omega_{coll}$

$I_{zz}\ \ddot{\psi} = K_\tau\ (\frac{540V_{coll} - \dot{\omega_{coll}}}{6})\ l_{boom} \sin(\phi) - K_v\ \dot{\psi}\ l_{boom} \sin(\phi) - K_D\ \dot{\psi}\ l_{boom} \cos(\gamma)$
$I_{zz}\ \ddot{\psi} = \frac{540V_{coll}\ K\tau\ l_{boom} \sin(\phi)}{6} - \frac{\dot{\omega_{coll}}\ K\tau\ l_{boom} \sin(\phi)}{6} - K_v\ \dot{\psi}\ l_{boom} \sin(\phi) - K_D\ \dot{\psi}\ l_{boom} \cos(\gamma)$

Re-arrange and preform Laplace Transformation:

$I_{zz}\ \ddot{\psi} + K_v\ \dot{\psi}\ l_{boom} \sin(\phi) + K_D\ \dot{\psi}\ l_{boom} \cos(\gamma) = = \frac{540V_{coll}\ K\tau\ l_{boom} \sin(\phi)}{6} - \frac{\dot{\omega_{coll}}\ K\tau\ l_{boom} \sin(\phi)}{6}$

$\Psi(s)\, I_{zz}\, s^2 + \Psi(s)\, K_v\, l_{boom} \sin(\phi)\, s + \Psi(s)\, K_D\, l_{boom} \cos(\gamma)\, s = \frac{540 V_{coll}\, K\tau\, l_{boom} \sin(\phi)}{6} - \frac{\omega_{coll}\, K\tau\, l_{boom} \sin(\phi)}{6}$

Applying small angle approximations: $\cos(n) \approx 1 \quad \sin(n) \approx n$

$\Psi(s)\, I_{zz}\, s^2 + \Psi(s)\, K_v\, l_{boom}\, s + \Psi(s)\, K_D\, l_{boom}\, s = \frac{540 V_{coll}\, K\tau\, l_{boom}\, \phi}{6} - \frac{\omega_{coll}\, K\tau\, l_{boom}\, \phi}{6}$

Preform Factorisation:

$\Psi(s)\, [I_{zz}\, s^2 + K_v\, l_{boom}\, \phi\, s + K_D\, l_{boom}\, s] = \frac{540 V_{coll}\, K\tau\, l_{boom}\, \phi - \omega_{coll}\, K\tau\, l_{boom}\, \phi}{6}$

Therefore, the transfer function, is as following:

$$G_{\Psi}(s) = \frac{90 V_{coll}\, K\tau\, l_{boom}\, \phi - \frac{\omega_{coll}\, K\tau\, l_{boom}\, \phi}{6}}{s^2(I_{zz}) + s(k_v l_{boom} \phi + k_D l_{boom})}$$

Fig.3 presents a flow chart of the augmented controller, which includes a main hub, alongside 2 sub-systems, which are situated within the Quanser block system.

This whole system is governed by 3 main expressions:

[A]; $G_{travel}\,(S) = \frac{\Psi\,(S)}{\phi_{command}}$

[B]; $G_{pitch}\,(S) = \frac{K_{pitch}}{I_{yy}(S)^2 + Damping\ Coefficients}$

[C]; $G_{roll}\,(S) = \frac{K_{pitch}}{I_{xx}(S)^2 + Damping\ Coefficients}$

Main hub [1]; The main hub will operate as the fundamental control system, incorporating both theta and roll angle (psi corrected) sub system, via the usage of a Quanser dynamics block. It overall function is give out a travel angle, in considerations of roll angle as well as theta (no direct influence). It serves a purpose in correcting the error between the command Ψ and the actual Ψ (travel) angle input. In-order to reduce error in control signals V_{cyc} & V_{coll}, a configured PDI controller is employed; looping to reduce error. These signals are then fed into the Quanser dynamics block.

Subsystem Pitch [2]; The prime focus for this subsystem within the Quanser dynamics block is to control pitch angle. It executes an PDI corrected signal of V_{coll} to adjust the collective rotor as well as stabilising vertical motion.

Subsystem Roll [3]; This subsystem focuses on manging both roll angle and yaw angle. Its has V_{cyc} being fed within its system, which also has been correct via an PDI. The sub system focuses on achieving a lateral stability and provide yaw coordination. Through an additional PDI controller it ensures roll error is at its minimum.

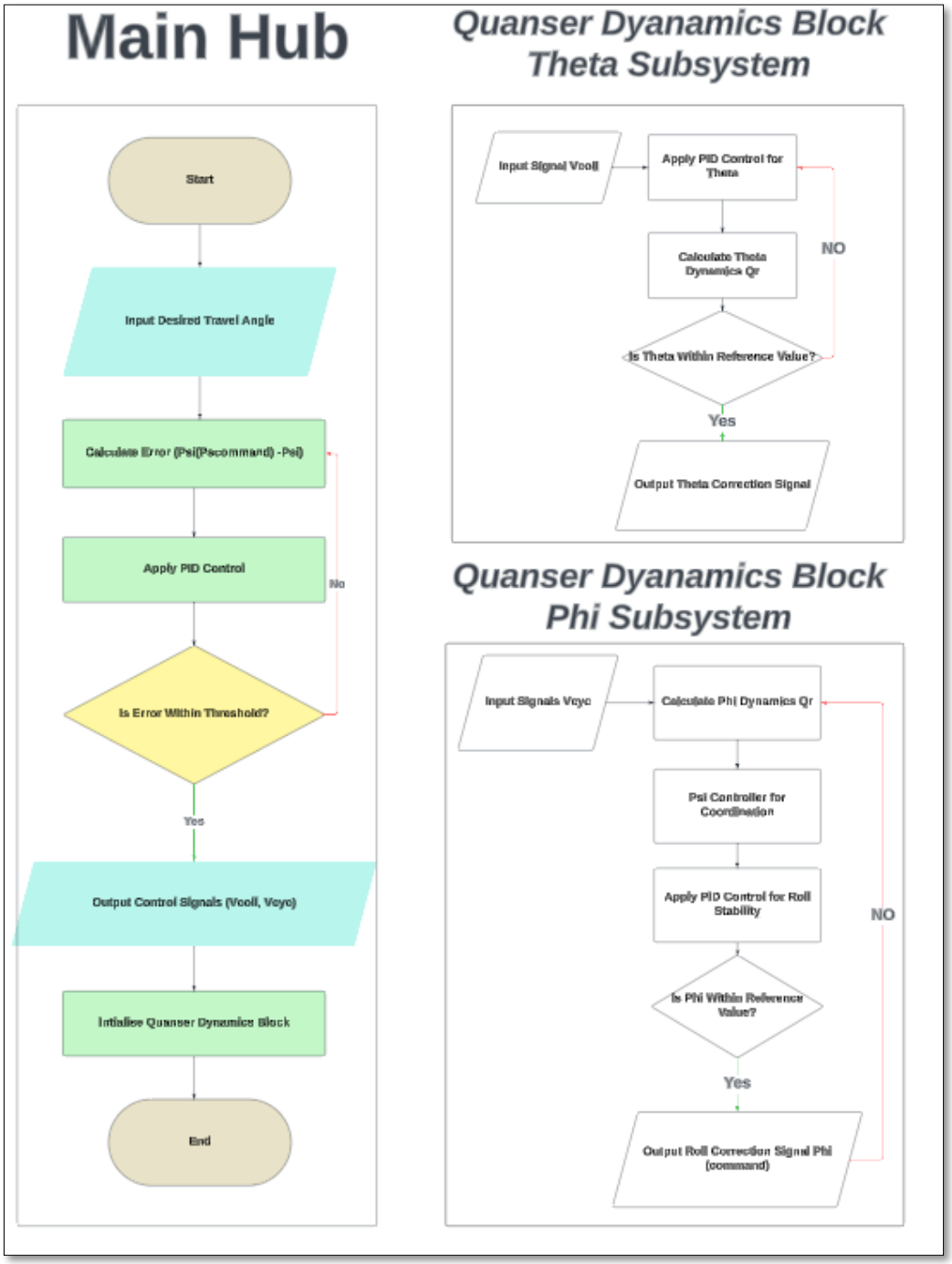

Figure 3 Flowchart for the Augmented Controller

[2.2] Design and Analysis of a Classical Travel vs (Psi) Controller:

The following section will now build on the foundations laid in augmented plant dynamics, discussed previously. This is achieved via designing a classical travel controller, in order to achieve precise control over the travel angle dynamics.
Emphasis on the design and analysis of a classical controller for the travel plant $G_{travel}(s)$, will involve the development as well as the analysis of a travel controller with explicit focus on the open-loop and closed-loop system behaviours, simulated step responses, and performance metrics such as stability and error margins.

For the next following tasks, there are 2 crucial formulas to establish:

[1] $G_{OL}\ (S) = \ G_c(S)\ G_P(S)$
Here the open-loop transfer function is the product of the controller transfer function $G_c(S)$ and the plant transfer function, $G_P(S)$.

[2] $G_{CL}\ (S) = \ \frac{G_{OLS}(S)}{1+\ G_{OL}(S)\ H(S)}$
Here the closed-loop transfer function includes the feedback and describes the relationship between the input and output of the system, $G_{CL}\ (S)$.

An mathematical model of the PID controller, manual tuned, presents itself with the following expressions;

[3] PID Open Loop Transfer function:

$G_{OL}\ (S) = \ G_c(S)\ G_P(S)$, where $G_c(S)$ is the following:

$G_c(S) = K_p + \frac{K_i}{s} + K_d\ \frac{N}{1+\frac{N}{S}}$, therefore: $G_{OL}\ (S) = (K_p\ +\ \frac{K_i}{s}\ +\ K_d\ \frac{N}{1+\frac{N}{S}},)\ G_P(S)$

[4] PID Closed Loop Transfer function:

$$G_{CL}\ (S) = \ \frac{G_{OLS}(S)}{1+\ G_{OL}(S)} = \frac{(K_p + \frac{K_i}{s} + K_d \frac{N}{1+\frac{N}{S}})}{1+(K_p + \frac{K_i}{s} + K_d \frac{N}{1+\frac{N}{S}})}$$

[2.2.1] Bode Plot of the Controller:

To proceed with the bode plot of the controller, the setup present on fig.1 and fig.2 remain the same, in which all feedback loops are intact. The closed-loop Bode plot effectively demonstrates the frequency response of the entire system, which includes, the PID controller as well as the Quanser dynamics block.
-Figure 3 represents the bode plot of the PID controller encapsulated within the Quanser block. This visualization highlights the controller's contribution to the system, in which it focuses on the response characteristics before its interaction with the PSI controller.
-Figure 4 likewise represents the bode plot of the classical PID controller prior to integration with the PSI controller. This intermediate step is critical for understanding how the PID controller tunes the iterative process, in order to achieve a both stable and accurate control of the Quanser system.
The combined use of these figures 3 & 4 illustrates the iterative tuning process as well as the frequency response characteristics of the system which allows for an in-depth evaluation of the controller's performance under closed-loop operation.

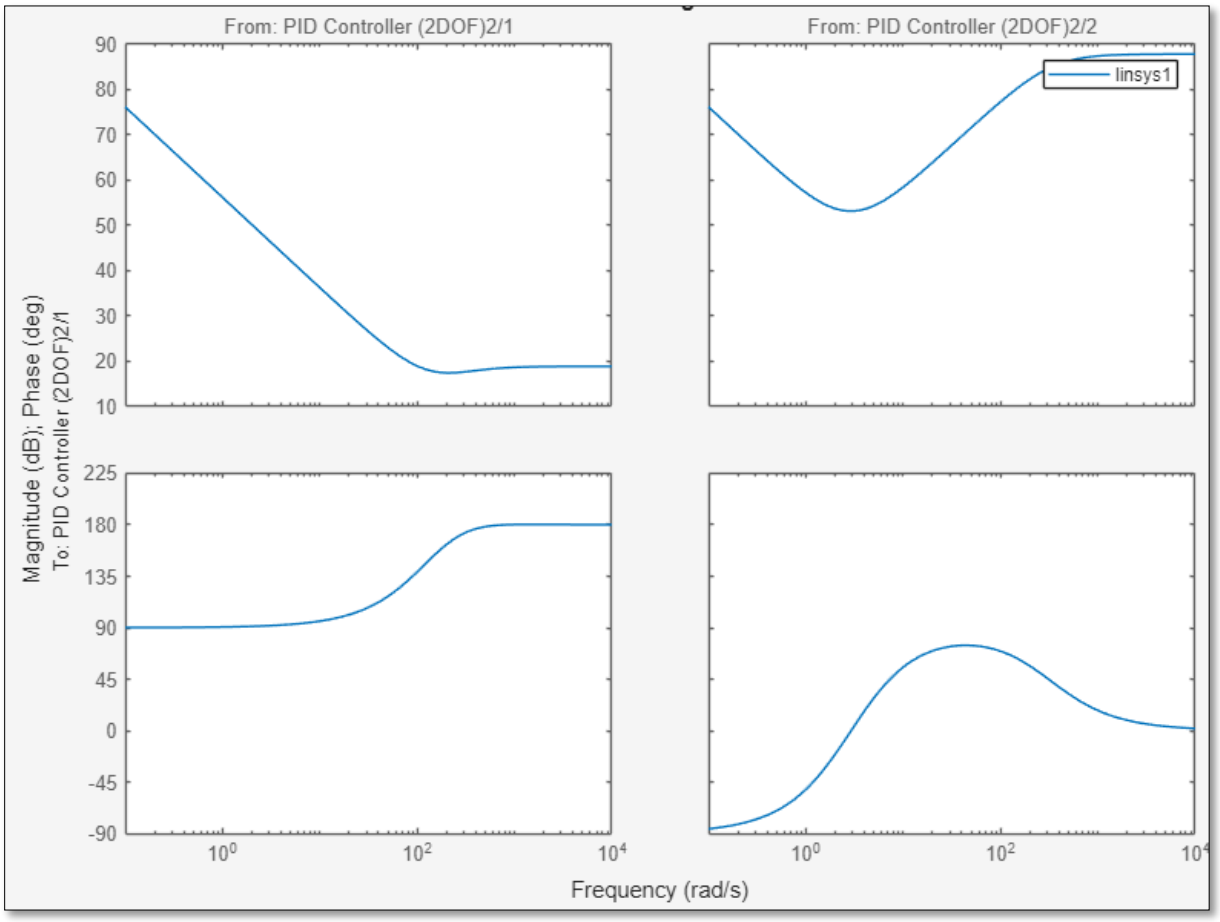

Figure 4. Bode plot for classical controller

The following bode plot (fig.4) represents the PID controller's frequency response as it operates within the Quanser dynamics block in Simulink.

The magnitude plot indicates how the controller amplifies signals at varying frequencies; simultaneously the phase plots demonstrate how the controller shifts the phase of signals. The gradual roll off in the magnitude response at higher frequencies as shown above, suggests the controller is effective when faced with high frequency noise; showcasing its ability to maintain stability.
The phase margin and gain margin, inferred from this graph, reflect the controller's stability when integrated with the system.

The plot below (fig.5) represents the PID controller's response prior to its interaction with the PSI controller. It also highlights the tuning adjustments via PID as well as the iterative improvements applied to the controller.

Evidently there seems to be smoother phase and magnitude transitions in this plot, which is suggesting that the system is able to achieve better tracking, and therefore a reduced sensitivity to disturbances, within the desired frequency range.

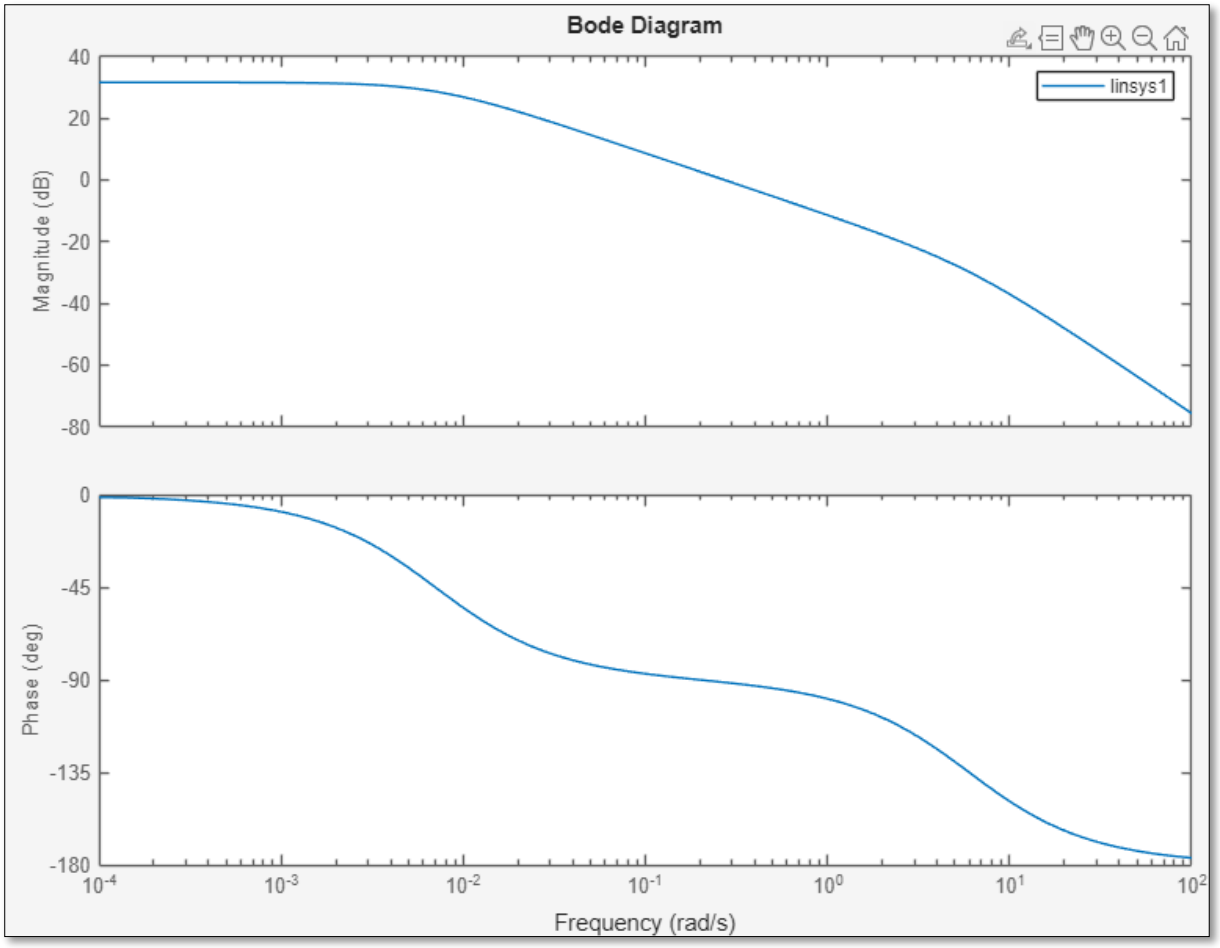

Figure 5. Bode plot for classical controller

[2.2.2] Open-Loop Bode Plot of the Controller + Plant

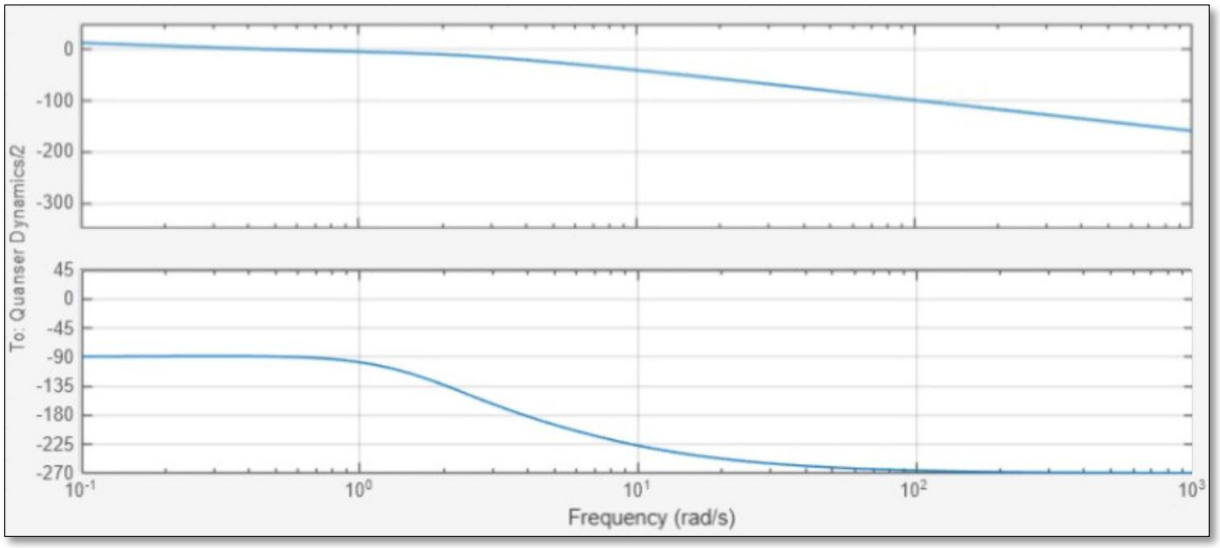

Figure 2. Bode plots for open loop Quanser Controller Plant

The open loop Bode plot presented in fig.5 depicts the frequency response of the combined Quanser Controller + Plant system without any feedback applied.

- Magnitude Plot; presented on the top view

The magnitude plot decreases steadily as frequency increases, which shows the system's attenuation at higher frequency signals.
This behaviour also indicates that the controller as well as the plant are designed to prioritize tracking low to mid frequency region signals; while simultaneously suppressing high frequency disturbances; this is considered to be a critical feature for stability and noise rejection. The magnitude at low frequencies remains relatively high; which likewise aligns with the system's ability to track low-frequency commands effectively. However, it is clearly visible how closed loop schematic present on fig.5, has a faster convergence then open loop; which was an prior prediction for model acceptability.

- Phase Plot; presented on the bottom view

The phase starts at approximately -90° and further decreases as the frequency increases. This steep drop-off in phase at higher frequencies indicates a potential phase lag; which may be the cause of no stability margins, which is the case in an open loop system; another prior prediction for model acceptability.

The phase response helps in evaluating how well the system is able to maintain stability under different fed frequency inputs.
The crossover frequency (where the gain magnitude crosses 0 dB) is not immediately apparent but is crucial for stability and performance, but as shown through annotation it produces a phase margin of nearly 90 degrees, which is considered to showcase a good level of stability, despite it being an open closed loop system (non-feedback loop).

In regards to the set up of this specific system, all feedback loops, where extracted from the model present in Fig.1 as well as its subsystem fig.2; which is the crucial step in creating a open loop, given it has no more feedback going into the PID, and therefore the model doesn't take into account error.

[2.2.3] Simulated Step Response for a 20º Step Command in Travel Angle

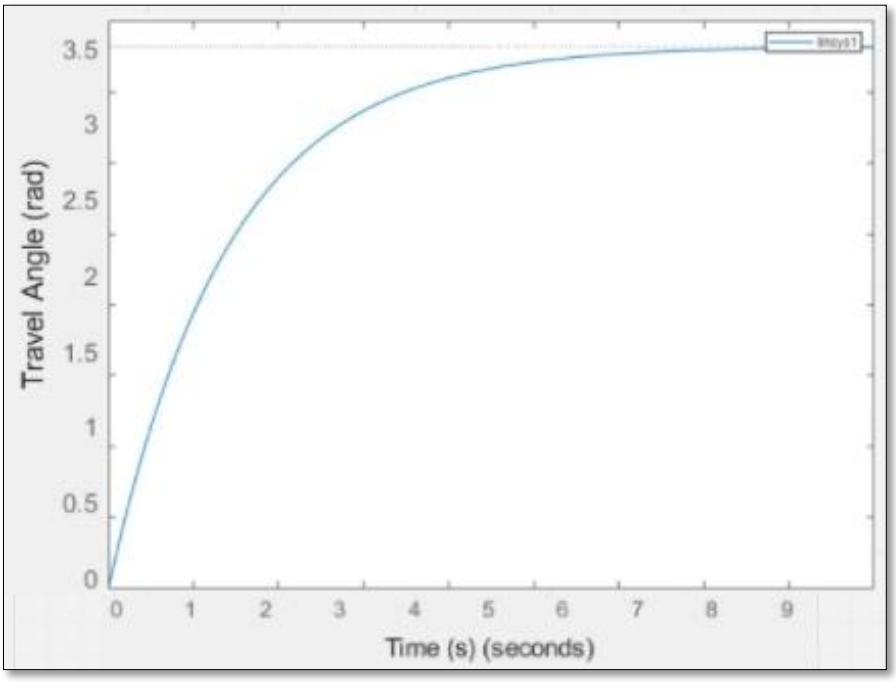

Figure 3. 20 degree step function (0.34 rad/s) travel angle

The system output converges to the desired travel angle of 0.34 rad/s
as indicated via the horizontal dashed line representing the target angle.
This demonstrates that the system is capable of accurately reaching as well as maintaining the commanded travel angle (via constant step input block)
The response shows a gradual increase in travel angle in which the system reaches approximately 90% of the target value within a time frame of 6 seconds. This rise time indicates a moderate responsiveness, in which case is suitable for ensuring stability as well as avoiding excessive overshoot.
The response however does not exhibit significant overshoot. This implies a well damped system; manual tuning via PID controllers. Tuning in this system was crucial as it prevented instability as well as maintaining smooth operation.
The response stabilizes without oscillations, highlighting the system's inherent stability and the effectiveness of the control strategy implemented.

[2.2.4] Simulated Step Response for a 20^{o} Step Command in Travel Angle

Pros/Cons:

Advantages of design	**Disadvantages of design**
Simplicity and Intuition: Easy to understand and implement.	**Limited to Linear Control**: Not ideal for multi-variable or highly nonlinear systems.
Real-Time Performance: Suitable for real-time applications with low computational needs.	**Integral Windup**: Can cause overshoot and instability if not handled properly.
Adjustable Performance: Gain parameters (P, I, D) provide flexibility in tuning.	**Lack of Robustness**: Not robust to parameter changes or system uncertainties.

[2.3.1] Open-Loop Bode Plot of the Controller (LQR +LQE)

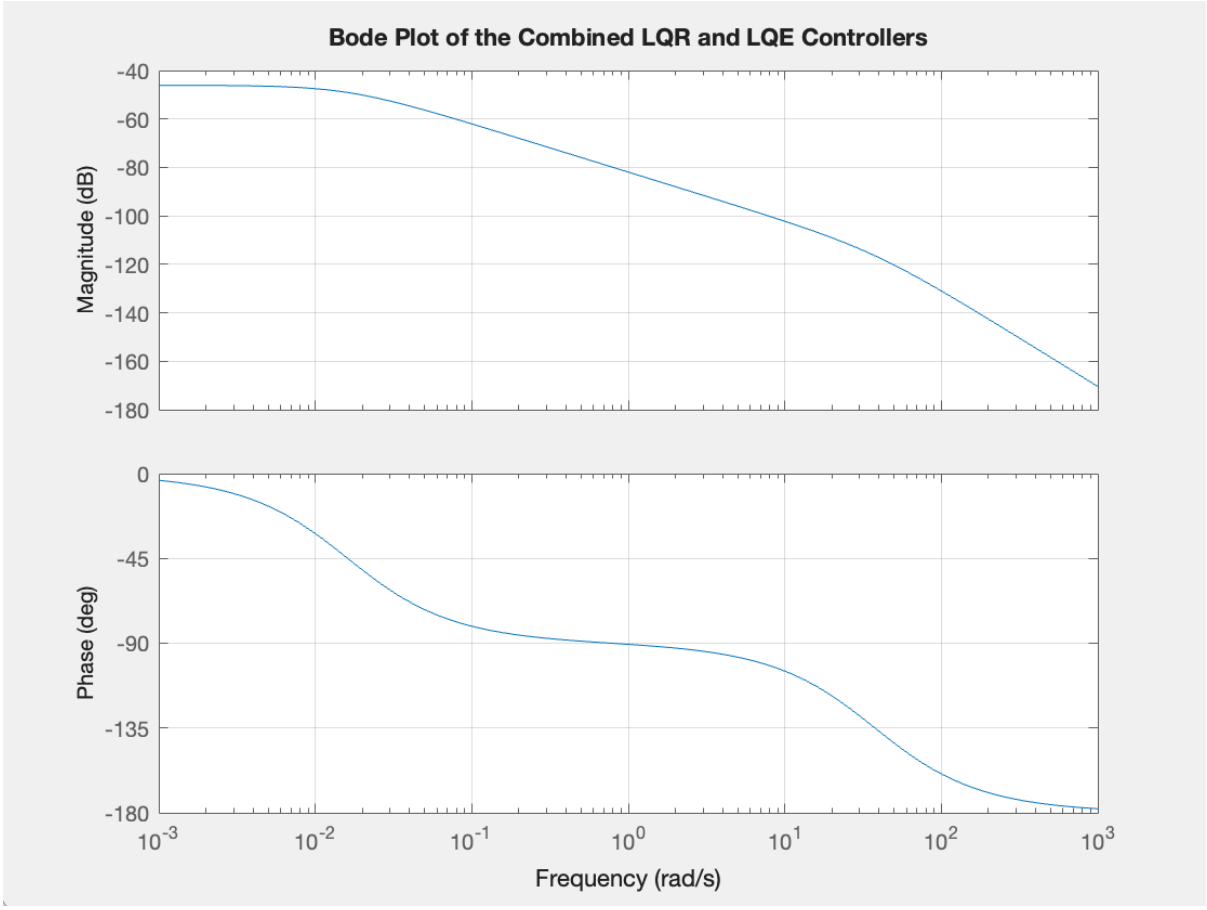

[2.3.2] Open-Loop Bode Plot of the Controller + Plant

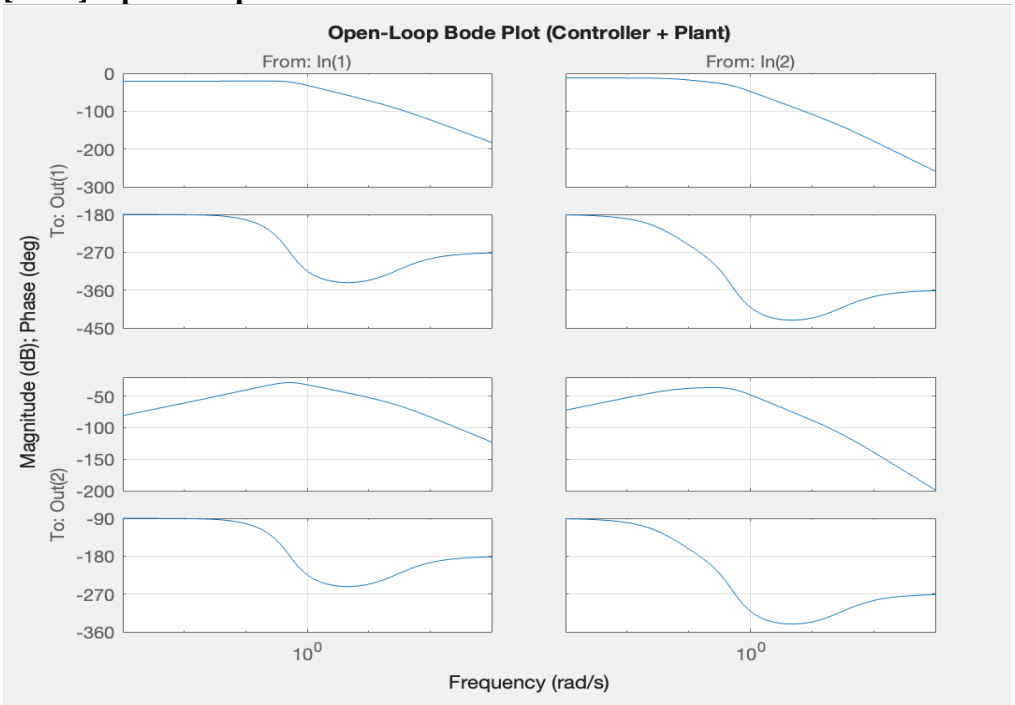

[2.3.3] Simulated Step Response for a 20º Step Command in Travel Angle

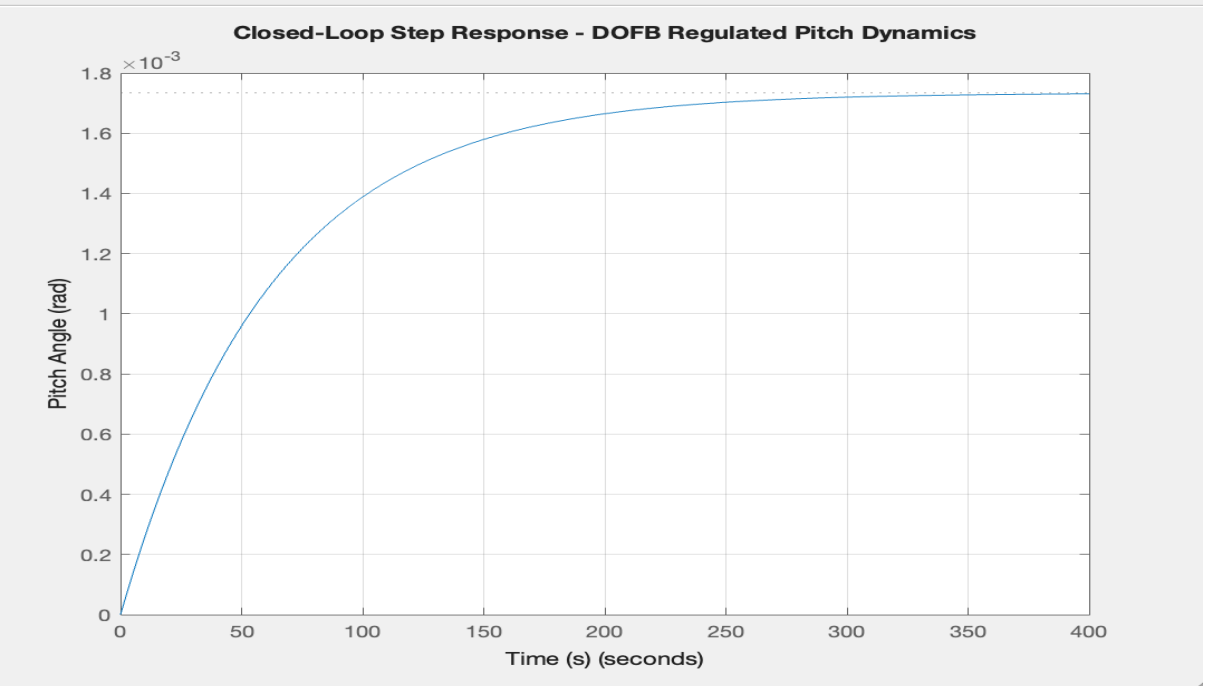

[2.3.4] Simulate the effect of small sensor noise on your controller to predict the flight test performance:

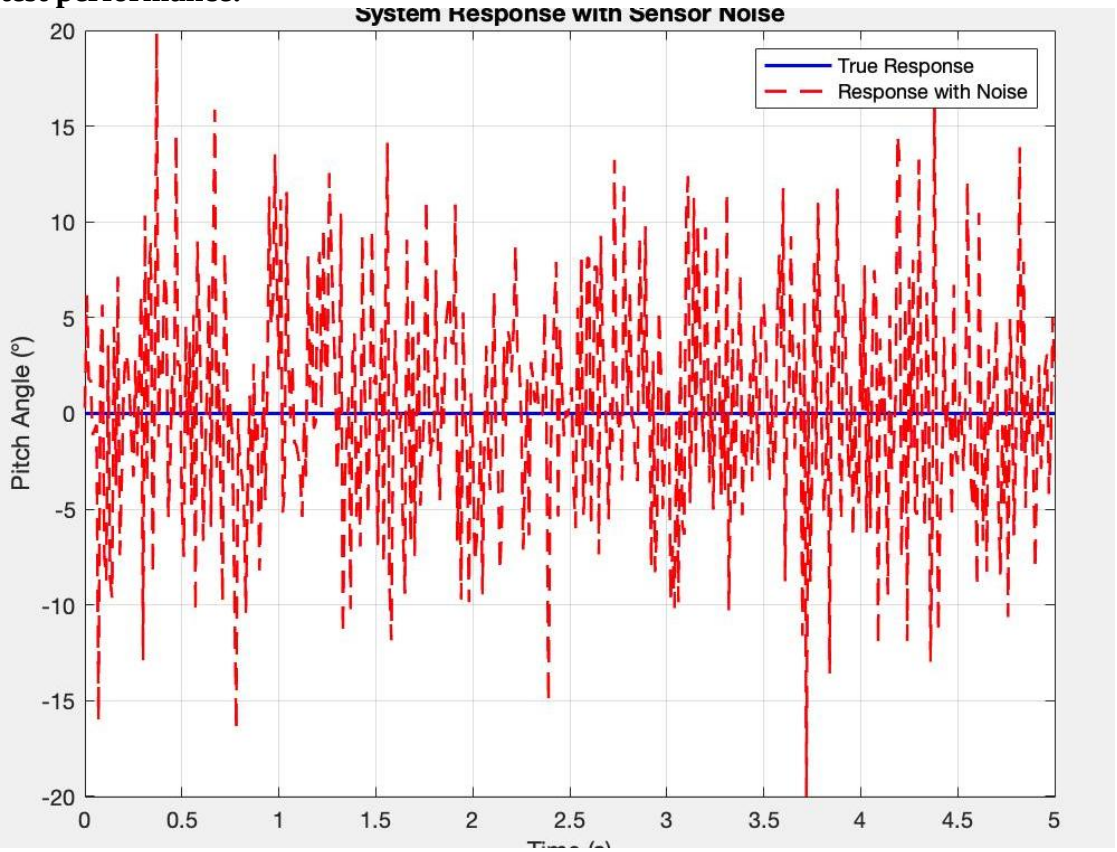

[2.3.5] A paragraph or two for design strategy, predict performance and pros/cons of

Our design:

Design strategy:
While solving for dynamics problems for continuous system is quite difficult. There are few general cases where solutions are accessible.

LQR (Linear Quadratic Regulator

The linear quadratic regulator is one of the most optimal dynamic feedback controllers up to date. LQR optimizes the dynamics performance feedback by minimizing the quadratic cost function [5]. Its basic duty is to balance the trade-off between control effort and the deviation of the states from desired trajectories. LQR solves the algebraic Ricatti's equation to have a gain matrix **K** that expresses the control law the equation for control law is given by.

$$\boldsymbol{u(t) = -k \cdot x(t)}$$

The Dynamic feedback provided by the LQR enables precise control of the Roll, Pitch and yaw trajectories in face of external disturbances. Unlike traditional controller which may control each degree of freedom separately, LQR can control the integrated inputs that can be represented as superior control. In addition to that, when it comes to noise and robustness, it automatically accounts for them like in the case of 3DOF Qaunser.

LQE (Linear Quadratic Estimator)
Qaunser , in case of control dynamics when some of the states are not directly measurable than these states are estimated. Similar to LQR, it minimizes the cost function and calculates the Observer Gain matrix **L.** using these matrix, it estimates the states x. When combined with the LQR, LQE behaves as the estimator which estimates some of the states in the coupled axes and allows the former to use these estimates for its calculation of gain matrix **K.** This combination is referred as **Linear Quadratic Gaussian (LQG).**

Basic Formula:

LQR:

$$\boldsymbol{u(t) = -k \cdot x(t) - state\ feedback}$$

The cost function for LQR is defined as;

$$\boldsymbol{J}=\int(\boldsymbol{x}^{\mathrm{T}}\cdot\boldsymbol{Q}\boldsymbol{x}+\boldsymbol{u}^{\mathrm{T}}\boldsymbol{R}\boldsymbol{u})\,\boldsymbol{d}\mathrm{t}$$

- Q is the semi-infinite matrix penalizing the state deviation from desired values
- R is the positive definitive matrix penalizing the control effort

LQE:

$$\dot{\boldsymbol{x}}(\mathrm{t})=\boldsymbol{A}\hat{\boldsymbol{x}}+\boldsymbol{B}\boldsymbol{u}(\boldsymbol{t})+\boldsymbol{L}(\boldsymbol{y}(\boldsymbol{t})-\hat{\boldsymbol{x}}(\boldsymbol{t}))$$

LQE minimizes the error covariance matrix P by solving the Ricatti's equation given below:

$$\boldsymbol{A}\boldsymbol{P}+\boldsymbol{P}\boldsymbol{A}^{\mathrm{T}}-\boldsymbol{P}\,\boldsymbol{C}^{\mathrm{T}}\,\boldsymbol{R}^{-1}\,\boldsymbol{C}\boldsymbol{P}+\boldsymbol{Q}=\boldsymbol{0}$$

Performance Prediction:
Robustness: The system is resistant to modelling uncertainties if the phase margin is at least 45° and the gain margin is high enough.
Noise Sensitivity: The controller seems to successfully suppress noise with a consistent roll-off at high frequencies.

Response Speed: A crossover frequency of about 1 rad/s suggests that the system may respond at a reasonable rate, which is appropriate for practical uses but not too fast.
Stability: If there are no 0 dB crossings at or below the −180° phase, the system seems stable.

Pros/Cons:

Advantages of design	**Disadvantages of design**
Optimal Performance: LQG being a combination of state estimation and optimal control is very precise for even noisy environments.	**Linear Dynamics**: it assumes system dynamics to be linear. Thus, it may not be able to fully capture the non-linearities in the system
Noise Handling: LQE estimator handles the noise efficiently and allows accurate state feedback.	**Computational Complexity**: The design for LQG can be computationally expensive, especially when it's a higher order system
Dynamic Adaptability: LQE can dynamically adapt to different noise levels when estimating noisy states.	**Tuning Expertise**: LQG demands careful tuning for the weighting matrices and covariance matrices.

[2.3.6] Comparison of DOFB Pitch Controller and the classic controller:

Classic interpretation:
If we consider classic interpretation, DOFB excels from the traditional controllers and handle systems that are more complex and tightly coupled. For high-order or multivariable systems, DOFB offers greater adaptability than traditional PID and Lead-Lag designs, despite their superior simplicity.

Classic	**DOFB**
Classic controllers are mostly done in the frequency domain	DOFB controller mostly operate in the state space domain
Scope of classic controller mostly lies with SISO (single input single output)	When it comes to MIMO (multi-input and multi output), DOFB controllers come into play
Classic controllers are mostly straight forward with transfer functions	DOFB controllers usually depends on solving for Ricatti's equation and estimates multiple states which are not directly available.
In terms of adaptability, classic mostly be useful for linear, time-invariant systems	These can be robust for the dynamics and uncertain systems

References

2 DOF helicopter - Quanser (2023). https://www.quanser.com/products/2-dof-helicopter/. (Fig.2., 2 DOF helicopter - Quanser, 2023)

Operations, A. and Operations, A. (2024) What are the "6 Degrees of Freedom"? 6DOF explained. https://industrial-ia.com/what-are-the-6-degrees-of-freedom-6dof-explained/. (Fig.1., - 6 Degrees Of Freedom)

CW Project: Quanser Helicopter, Dr Abdelhafid Zenati (Fig.3., - Quanser Helicopter Travel Yaw.Angle (ψ)

CW Project: Quanser Helicopter, Dr Abdelhafid Zenati (Fig.4., - Quanser Helicopter Roll (φ) Angle with Rotor Forces)

CW Project: Quanser Helicopter, Dr Abdelhafid Zenati (Fig.5., - Quanser Helicopter Pitch (θ) Angle with Support Stand)

2 DOF helicopter - Quanser (2023). https://www.quanser.com/products/2-dof-helicopter/. (Fig.6., Pitch Control System)

2 DOF helicopter - Quanser (2023). https://www.quanser.com/products/2-dof-helicopter/. (Fig.7., Roll Control System)

2 DOF helicopter - Quanser (2023). https://www.quanser.com/products/2-dof-helicopter/. (Fig.6., Pitch Control System)

3 DOF helicopter - Quanser (2023). https://www.quanser.com/products/3-dof-helicopter/.

Zenati, A., 2024. CW Project: Quanser Helicopter. *PowerPoint presentation, City University of London.*

uk.mathworks.com. (n.d.). Control Systems in Practice: What are Transfer Functions? [online] Available at: https://uk.mathworks.com/videos/what-are-transfer-functions-1661846920974.html.

Ogata, K. (2010). *Modern Control Engineering* (5th ed.). Pearson Education.

Nise, N. S. (2011). *Control Systems Engineering* (6th ed.). Wiley.

Astrom, K. J., & Hagglund, T**.** (2006). *PID Controllers: Theory, Design, and Tuning* (2nd ed.). ISA - The Instrumentation, Systems, and Automation Society.

Gawthrop, P., & Smith, L. (2011). *The Theory and Application of PID Controllers* in *Control Engineering Practice*.

Mehmet, A., & Yılmaz, E. (2016). "Application of PID control for altitude and attitude stabilization of unmanned aerial vehicles." *International Journal of Control and Automation*, 9(12), 9-18.

Liu, H., & Wang, Q**.** (2014). "Design and implementation of a PID controller for roll and pitch control of a quadcopter." *2014 IEEE International Conference on Automation and Logistics* (ICAL).

Umich.edu. (2023). *Control Tutorials for MATLAB and Simulink - Introduction: PID Controller Design*. [online] Available at: https://ctms.engin.umich.edu/CTMS/index.php?example=Introduction&section=ControlPID#13.